Alkaline Lyotropic Silicate−Surfactant Liquid Crystals

A. Firouzi,‡ F. Atef,‡ A. G. Oertli,‡,† G. D. Stucky,§ and B. F. Chmelka*,‡

Contribution from the Department of Chemical Engineering, Department of Chemistry, and Materials Department, University of California, Santa Barbara, California 93106

Received August 26, 1996. Revised Manuscript Received January 22, 1997[⊗]

Abstract: Multinuclear (^{2}H, ^{13}C, ^{29}Si, ^{81}Br) magnetic resonance spectroscopy, small-angle X-ray scattering, and polarized optical microscopy techniques have been used to investigate molecular and mesoscopic organization in silicate−surfactant lyotropic liquid crystals with hexagonal and lamellar morphologies under highly alkaline conditions. Such systems cooperatively self-assemble following the addition of a basic aqueous solution containing anionic silicate oligomers (e.g., double-four-ring species) to an isotropic micellar solution of cationic surfactant molecules (e.g., cetyltrimethylammonium bromide). Important similarities and differences are shown to exist between multicomponent silicate−surfactant and conventional binary lyotropic liquid crystals. Under highly alkaline conditions, the silicate−surfactant systems possess the characteristics of ordinary lyotropic liquid crystalline systems, though the balance of forces underlying their self-assembly is complicated by the richness of the aqueous silicate chemistry. This is the first comprehensive description of lyotropic silicate−surfactant liquid crystalline behavior, from which detailed insight is obtained into the molecular factors governing inorganic−organic mesophase formation in aqueous media.

Introduction

A great deal of attention is currently being paid to the synthesis of novel chemical systems containing mixed inorganic and organic components, the goal of which is usually to achieve some blend of desirable macroscopic properties in the composite or final product material. Examples of such increasingly varied systems include zeolite and mesoporous molecular sieves,[1−14] biominerals,[15] and analogous heterogeneous polymeric mix-tures,[16] whose properties can be modified according to the composition and conditions of a typically complicated multi-component mixture. To design and control the organization, composition, and resultant properties of such composite inor-ganic−organic systems, a firm physicochemical understanding is necessary of the structure and dynamics of the component species that are responsible for local, mesoscopic, and/or long-range order in these materials.

In a number of aqueous inorganic−organic systems, the organic species act as structure-directing agents through coop-erative interactions with the inorganic component across a hydrophobic−hydrophilic interface. For example, the discovery[1a,b] that alkaline anionic silicate−cationic surfactant mixtures could be used to produce mesoporous solids with uniform tunable pore dimensions has initiated widespread efforts to control and expand such synthesis strategies to a large number of inorganic−

‡ Department of Chemical Engineering.
† Present address: Ciba-Geigy Ltd., CH-4002 Basel, Switzerland.
§ Department of Chemistry and Materials Department.
⊗ Abstract published in *Advance ACS Abstracts,* March 15, 1997.
(1) (a) Kresge, C. T.; Leonowicz, M. E.; Roth, W. J.; Vartuli, J. C.; Beck, J. S. *Nature* **1992,** *359,* 710−712. (b) Beck, J. S.; Vartuli, J. C.; Roth, W. J.; Leonowicz, M. E.; Kresge, C. T.; Schmitt, K. D.; Chu, C. T-W.; Olson, D. H.; Sheppard, E. W.; McCullen, S. B.; Higgins, J. B.; Schlenker, J. L. *J. Am. Chem. Soc.* **1992,** *114,* 10834−10843. (c) Beck, J. S.; Vartuli, J. C.; Kennedy, G. J.; Kresge, C. T.; Roth, W. J.; Schramm, S. E. *Chem. Mater.* **1994,** *6,* 1816−1821.
(2) Monnier, A.; Schüth, F.; Huo, Q.; Kumar, D.; Margolese, D. I.; Maxwell, R. S.; Stucky, G. D.; Krishnamurty, M.; Petroff, P.; Firouzi, A.; Janicke, M.; Chmelka, B. F. *Science* **1993,** *261,* 1299−1303.
(3) (a) Huo, Q.; Margolese, D. I.; Ciesla, U.; Demuth, D. G.; Feng, P.; Gier, T. E.; Sieger, P.; Firouzi, A.; Chmelka, B. F.; Schüth, F.; Stucky, G. D. *Chem. Mater.* **1994,** *6,* 1176−1191. (b) Huo, Q.; Margolese, D. I.; Ciesla, U.; Feng, P.; Gier, T. E.; Sieger, P.; Leon, R.; Petroff, P. M.; Schüth, F.; Stucky, G. D. *Nature* **1994,** *368,* 317−321.
(4) (a) Huo, Q.; Leon, R.; Petroff, P. M.; Stucky, G. D. *Science* **1995,** *268,* 1324−1327. (b) Huo, Q.; Margolese, D. I.; Stucky, G. D. *Chem. Mater.* **1996,** *8,* 1147−1160.
(5) Firouzi, A.; Kumar, D.; Bull, L. M.; Besier, T.; Sieger, P.; Huo, Q.; Walker, S. A.; Zasadzinski, J. A.; Glinka, C.; Nicol, J.; Margolese, D. I.; Stucky, G. D.; Chmelka, B. F. *Science* **1995,** *267,* 1138−1143.
(6) Firouzi, A.; Stucky, G. D.; Chmelka, B. F. *Synthesis of Microporous Materials*; Occelli, M. L., Kessler, H., Eds.; Marcel Dekker, Inc.: New York, 1996; pp 379−389.
(7) (a) Chen, C. Y.; Li, H. X.; Davis, M. E. *Microporous Mater.* **1993,** *2,* 17−26. (b) Chen, C. Y.; Burkett, S. L.; Li, H. X.; Davis, M. E. *Microporous Mater.* **1993,** *2,* 27−34. (c) Chen, C. Y.; Xiao; S. Q.; Davis, M. E. *Microporous Mater.* **1995,** *4,* 1−20.
(8) (a) Tanev, P. T.; Pinnavaia, T. J. *Science* **1995,** *267,* 865−867. (b) Tuel, A.; Gontier, S. *Chem. Mater.* **1996,** *8,* 114−122. (c) Attard, G. S.; Glyde, J. C.; Göltner, C. G. *Nature* **1995,** *378,* 366−368.
(9) Fyfe, C. A.; Fu, G. *J. Am. Chem. Soc.* **1995,** *117,* 9709−9714.
(10) (a) Cheng, C.; Luan, Z.; Klinowski, J. *Langmuir* **1995,** *11,* 2815−2819. (b) Steel, A.; Carr, S. W.; Anderson, M. W. *Chem. Mater.* **1995,** *7,* 1829−1832. (c) Steel, A.; Carr, S. W.; Anderson, M. W. *J. Chem. Soc., Chem. Commun.* **1994,** 1571−1572.

(11) Yang, H.; Kuperman, A.; Coombs, N.; Mamiche-Afara, S.; Ozin, G. A. *Nature* **1996,** *379,* 703−705.
(12) (a) Liu, J.; Kim, A. Y.; Virden, J. W.; Bunker, B. C. *Langmuir* **1995,** *11,* 689−692. (b) Wang, L.; Liu, J.; Exarhos, G. J.; Bunker, B. C. *Langmuir* **1996,** *12,* 2663−2669.
(13) (a) Vaudry, F.; Khodabandeh, S.; Davis, M. E. *Chem. Mater.* **1996,** *8,* 1451−1464. (b) Bagshaw, S. A.; Pinnavaia, T. J. *Angew. Chem., Int. Ed. Engl.* **1996,** *35,* 1102−1105. (c) Busio, M.; Jänchen, J.; van Hooff, J. H. C. *Microporous Mater.* **1995,** *5,* 211−218. (d) Kolodziejski, W.; Corma, A.; Navarro, M.; Pérez-Pariente, J. *Solid State Nucl. Magn. Reson.* **1993,** *2,* 253−259. (e) Alfredsson, V.; Keung, M.; Monnier, A.; Stucky, G. D.; Unger, K. K.; Schüth, F. *J. Chem. Soc., Chem. Commun.* **1994,** 921−922.
(14) (a) Antonelli, D. M.; Nakahira, A.; Ying, J. Y. *Inorg. Chem.* **1996,** *35,* 3126−3136. (b) Tanev, P. T.; Chibwe, M.; Pinnavaia, T. J. *Nature* **1994,** *368,* 321−323. (c) Reddy, K. M.; Moudrakovski, I.; Sayari, A. *J. Chem. Soc., Chem. Commun.* **1994,** 1059−1060. (d) Sayari, A.; Moudrakovski, I.; Danumah, C.; Ratcliffe, C. I.; Ripmeester, J. A.; Preston, K. F. *J. Phys. Chem.* **1995,** *99,* 16373−16379. (e) Zhao, D.; Goldfarb, D. *J. Chem. Soc., Chem. Commun.* **1995,** 875−876. (f) Ciesla, U.; Demuth, D.; Leon, R.; Petroff, P. M.; Stucky, G. D.; Unger, K. K.; Schüth, F. *J. Chem. Soc., Chem. Commun.* **1994,** 1387−1388.
(15) (a) Heywood, B. R.; Mann, S. *Adv. Mater.* **1994,** *6,* 9−20. (b) Mann, S. *Nature* **1993,** *365,* 499−505. (c) Archibald, D. D.; Mann, S. *Nature* **1993,** *364,* 430−433. (d) Weiner, S. *Crit. Rev. Biochem.* **1986,** *20,* 365−408. (e) Williams R. J. P. *Philos. Trans. R. Soc. London, Ser. B* **1984,** *304,* 411−424.
(16) (a) Antonietti, M.; Conrad, J.; Thünemann, A. *Macromolecules* **1994,** *27,* 6007−6011. (b) Antonietti, M.; Conrad, J. *Angew. Chem., Int. Ed. Engl.* **1994,** *33,* 1869−1870. (c) Judeinstein, P.; Sanchez, C. *J. Mater. Chem.* **1996,** *6,* 511−525. (d) Sarrazin-Cartalas, A.; Iliopoulos, I.; Audebert, R.; Olsson, U. *Langmuir* **1994,** *10,* 1421−1426.

surfactant materials.[3,13,14] However, the physics underlying these diverse chemical syntheses has remained poorly understood and elusive, largely because of the complicated nature of the multicomponent mixtures and often overlapping self-assembly and inorganic polymerization processes. Nevertheless, it has been shown that such syntheses involve highly cooperative interfacial interactions among the inorganic and organic components, which account for the mesophase self-assembly observed in these materials.[1−10] Furthermore, we have recently demonstrated that under conditions of low reactivity of silicate species at high pH and low temperatures, these complex mesophases possess characteristics common to conventional lyotropic liquid crystals.[5,6]

In this paper, molecular origins of the self-assembly, organization, and phase behavior of alkaline silicate−surfactant liquid crystals are examined for the first time in detail using a combination of complementary experimental techniques. These include ^{2}H, ^{13}C, ^{29}Si, and ^{81}Br nuclear magnetic resonance (NMR) spectroscopy, X-ray diffraction, and polarized optical microscopy measurements, which provide important structural information over molecular, mesoscopic, and macroscopic length scales. For a given mixture composition and temperature, various energetic contributions to the Gibbs free energy are balanced, with the result that, under conditions of thermodynamic equilibrium, a mesophase will self-assemble into the configuration with the lowest overall energy. Moreover, the presence of polymerizable silicate anions at the interfacial region of the silicate−surfactant mesophase introduces opportunities for further manipulation of the phase structure through condensation of the silicate species, which may be achieved by lowering the pH and/or increasing the temperature. In such cases, as silica polymerization progresses, the charge density of the inorganic framework is reduced, thereby altering the interfacial force balance. As a consequence of these non-equilibrium changes, the system may respond by adopting a new mesophase morphology, providing the flexibility of the cross-linking silicate network allows it.[5−7] Here, the emphasis is exclusively on the case where interfacial silicate polymerization is negligible, for which the self-assembled mesophases display lyotropic liquid crystalline behavior under conditions of thermodynamic equilibrium.

A characteristic of many surface-active (e.g., amphiphilic) molecules is that above their critical micellar concentration (CMC), they self-assemble into micellar aggregates. According to a microscopic model introduced by Israelachvili *et al.*,[17] which lends itself well to the molecular NMR measurements of this study, the preferred aggregate shape in the dilute regime depends on the effective mean molecular parameters that establish the value of a dimensionless packing parameter g defined as

$$g \equiv \frac{V}{a_{o}l_{c}} \tag{1}$$

where V is the effective volume of the hydrophobic chain, a_{o} is the mean aggregate surface area per hydrophilic head group, and l_{c} is the critical hydrophobic chain length.[17] The parameter g depends on the molecular geometry of the surfactant species, such as the number of carbon atoms in the hydrophobic chain, the degree of chain saturation, and the size or charge of the polar head group. In addition, the effects of solution conditions, including ionic strength (e.g., electrolyte concentration), pH, co-surfactant concentration, and temperature, are included implicitly in V, a_{o}, and l_{c}.[18] These account for various solution-dependent

intra-aggregate interactions that contribute to the adoption of a particular aggregate shape. Different aggregate shapes correlate with different ranges of g values, which can therefore be used to predict the influences of various molecular species on the phase behavior of a system. Strictly speaking, this molecular treatment is appropriate only when inter-aggregate interactions can be neglected.[19] Although this assumption is valid for dilute surfactant mixtures, such as micellar, vesicular, or microemulsion solutions, it is less appropriate for more concentrated amphiphile solutions in which the self-assembled aggregates adopt densely packed arrangements, such as mesoscopically ordered lyotropic liquid crystal (LLC) phases. Equation 1 is nevertheless helpful for predicting the relative stabilities of different aggregate shapes and the corresponding mesophase morphologies.

Mesoscopically ordered lyotropic liquid crystal phases can form under circumstances where either repulsive or attractive inter-aggregate interactions dominate, depending on solution conditions.[18] The former is often the case with conventional binary systems in the so-called weak-screening limit, where electrostatic repulsions predominate, resulting in single LLC mesophases that fill an entire sample volume. Conversely, in the strong-screening limit where high concentrations of ions and/or multivalent ions are present, attractive inter-aggregate interactions can dominate the repulsive contributions, so that a two-phase system may result. This situation can be induced, for example, by increasing the ionic strength or the pH of a surfactant solution, which reduces the characteristic Debye length of the diffusive double layer along with the corresponding surface potential of dispersed micelles. As a result, more effective screening of the double-layer electrostatic repulsion forces is achieved.[18] In addition, important attractive inter-aggregate interactions exist in the form of van der Waals forces among the surfactant molecules[20] and attractive ion-correlation van der Waals forces,[21] which act among highly mobile and polarizable counterions in the diffuse double layer. Thus, addition of electrolyte can cause the overall force balance to shift in favor of attractive interactions, causing a surfactant-rich mesophase to separate from a second solvent-rich isotropic phase.

We have recently argued that the domination of inter-aggregate attractive forces over their respective repulsive interactions is crucial to the self-assembly of silicate−surfactant lyotropic liquid crystals.[5,6] These mesophases are prepared under highly alkaline conditions from separate isotropic aqueous inorganic and surfactant precursor solutions containing multiply charged anionic silicate oligomers and cationic micelles, respectively. Specifically, the inorganic precursor solution consists primarily of double-four-ring (D4R) silicate oligomers that are multiply charged at high pH (13.0), while the dilute (1−20 wt %, above the critical micelle concentration CMC) organic precursor solution contains spherical or cylindrical micelles prepared using cetyltrimethylammonium bromide (CTAB), a cationic surfactant. The micelles can be swollen by adding organic solute molecules, such as benzene or trimethylbenzene, which have an effect analogous to an increase of the hydrophobic chain volume V in eq 1. As will be

(17) Israelachvili, J. N.; Mitchell, D. J.; Ninham, B. W. *J. Chem. Soc., Faraday Trans. 2* **1976**, *72*, 1525−1568.

(18) Israelachvili, J. N. *Intermolecular & Surface Forces*; Academic Press: London, 1991.

(19) Roux, D.; Coulon, C. *J. Phys.* **1986**, *47*, 1257−1264.

(20) (a) Marra, J. *J. Colloid Interfac. Sci.* **1985**, *107*, 446−458. (b) Marra, J. *J. Colloid Interfac. Sci.* **1986**, *109*, 11−20.

(21) (a) Wennerström H.; Jönsson B.; Linse P. *J. Phys. Chem.* **1982**, *76*, 4665−4670. (b) Guldbrand L.; Jönsson B.; Wennerström H.; Linse P. *J. Chem. Phys.* **1984**, *80*, 2221−2228. (c) Kjellander R.; Marčelja S.; Pashley R. M.; Quirk, J. P. *J. Phys. Chem.* **1988**, *92*, 6489−6492.

discussed in detail below, such silicate−surfactant systems phase separate, with at least one phase displaying liquid crystalline properties over a wide range of alkaline solution compositions and temperatures.

Silicate−surfactant liquid crystals, moreover, can also serve as intermediates in the organization and polymerization of inorganic networks, as in the preparation of mesoporous molecular sieves, which have been the object of much recent attention.[1−14] Although condensed inorganic−surfactant mesophases can be formed with numerous inorganic species,[3,13,14] with single- or multiple-tailed cationic or anionic surfactants,[3,4] with nonionic surfactants,[8] with covalently linked surfactant−metal molecules as precursors,[4b,14a] in concentrated surfactant solutions,[8c] and in acidic or basic media,[3] liquid crystalline characteristics have been observed under relatively narrow ranges of conditions, such as in the presence of stable ionic silicate species at high pH and low temperatures.[5,6] The absence of appreciable inorganic polymerization is expected to be a general prerequisite for observing liquid crystalline behavior in silicate−surfactant mesophases.

Experimental Section

The deuteration procedures of the cationic surfactant (cetyltrimethylammonium bromide) at the α-carbon and the head group positions are outlined below, followed by descriptions of the synthesis strategies for the formation of silicate−surfactant liquid crystals and a discussion of the various experimental techniques employed in the characterization of these materials.

Chemicals. The cationic surfactant used in this study was cetyltrimethylammonium bromide, $[C_{16}H_{33}N^+(CH_3)_3]Br^-$ (CTAB), the organic solutes were benzene and 1,3,5-trimethylbenzene (TMB), the sources of base were tetramethylammonium hydroxide (TMAOH) or tetraethylammonium hydroxide (TEAOH), and the co-solvents were methanol (CH_3OH) or ethanol (EtOH), all of which were purchased from Aldrich Chemical Co., Inc. The silica source was Cab-O-Sil M-5 (scintillation grade) obtained from Kodak Chemical Co. All chemicals were used as received.

α-Deuterated Cetyl Alcohol. To a solution of $LiAlD_4$ (6.8 g, 0.16 mol) in anhydrous ether (250 mL) was added dropwise a solution of palmitic acid (36 g, 0.14 mol) in anhydrous ether (250 mL), and the mixture was refluxed for 1 h. The reaction mixture was quenched with ice water (100 mL) and acidified with half-concentrated H_2SO_4. The organic phase was separated and dried over $MgSO_4$. After removing the solvent, the crude product was distilled at 100−120 °C (2 Torr). ^{1}H NMR (500 MHz, $CDCl_3$) δ 1.54 (t, 2H), 1.45 (s, 1H), 1.35−1.25 (m, 26H), 0.85 (t, 3H) ppm.

α-Deuterated Cetyl Bromide.[22] To a solution of deuterated cetyl alcohol (4.8 g, 19.7 mmol) in toluene (10 mL) was added PBr_5 (10.5 g, 24.4 mmol) in three portions, and the mixture was heated to 80 °C for 4 h. The resultant solution was poured onto ice and diluted with ether. The organic phase was separated and washed with 1 M NaOH (3×), 1 M HCl (3×), and water (3×), respectively. The ether was evaporated and the residue was distilled at 125−131 °C (0.7 Torr). ^{1}H NMR (500 MHz, $CDCl_3$) δ 1.84 (t, 2H), 1.42 (q, 2H), 1.35−1.25 (m, 24H), 0.88 (t, 3H) ppm.

α-Deuterated CTAB (CTAB-d_2).[22] To an ethanolic solution of $N(CH_3)_3$ (5.0 g, 35 wt % in ethanol, 29.7 mmol) was added deuterated cetyl bromide (4.0 g, 13.0 mmol) at ambient temperature. The mixture was stirred for 24 h, and the resultant precipitate was collected and recrystallized from ethanol/acetone (3×) and dried in vacuo at room temperature. ^{1}H NMR (500 MHz, $CDCl_3$) δ 3.48 (s, 9H), 1.74 (t, 2H), 1.37 (q, 2H), 1.35−1.25 (m, 24H), 0.88 (t, 3H) ppm.

Silicate−Surfactant Lyotropic Liquid Crystals at High pH. Typical silicate−surfactant lyotropic liquid crystal systems were prepared by combining dilute aqueous isotropic surfactant and silicate

precursor solutions as follows below. Aqueous micellar precursor solutions containing 5−12 wt % CTAB and varying amounts of organic solute, up to 0.8 M trimethylbenzene or benzene, were mixed and heated gently (40−50 °C) to dissolve the surfactant. The inorganic precursor solution was prepared by dissolving 6.0 g (0.1 mol) of Cab-O-Sil in 30 g of aqueous tetramethylammonium hydroxide (TMAOH) solution (25.0 wt %), 56 g of H_2O, and 45 g (1.4 mol) of methanol (CH_3OH).[23] The solution was heated at 70 °C for 24 h, so that a clear solution (pH 13.0) was obtained. The combination of TMAOH and CH_3OH is known to stabilize the double-four-ring (D4R) silicate oligomers,[23] with this mixture formulation yielding primarily the D4R species, as shown below. The overall molar composition of this D4R silicate precursor solution was $1.0SiO_2$:1.1TMAOH:42H_2O:14.1CH_3OH. Similarly, double-three-ring (D3R) silicate species can be preferentially stabilized[24] by dissolving 3.9 g (0.07 mol) of Cab-O-Sil in 100 g of aqueous tetraethylammonium hydroxide (TEAOH) solution (35 wt %) and 37 g (0.8 mol) of ethanol (EtOH) and heating at 70 °C for 24 h (pH 13.5). The overall molar composition of this predominantly D3R silicate precursor solution was $1.0SiO_2$:3.7TEAOH:56.2H_2O:12.3EtOH. Depending on the mesophase desired and the characterization technique employed, appropriate amounts of the surfactant and silicate precursor solutions were combined at room temperature and the samples stirred for 30 min to several days to allow equilibration. No spectroscopic changes were observed for longer times, indicating that equilibrium mixtures were obtained. Upon combining the surfactant and silicate precursor solutions, the pH of the mixtures studied here typically dropped half a pH unit below that of the initial pH of the silicate precursor solution.

NMR Spectroscopy. All NMR spectra were acquired at 11.7 T on a Chemagnetics CMX-500 spectrometer, except for the deuterium (^{2}H) measurements with [2]H_2O that were collected at 7.0 T on a General Electric GN-300 spectrometer. For the ^{2}H NMR measurements at 11.7 T, a standard quadrupolar-echo pulse sequence was used with π/2 pulses of 4−6 μs, a 50-μs echo delay, a recycle delay of 0.25 s, and 3600−7200 signal acquisitions. Samples containing deuterated surfactant species were measured using specially designed 10-mm Kel-F containers with threaded caps to prevent the loss of solvent or organic solute during heating. For the [2]H_2O NMR measurements at 7.0 T, 900 scans were acquired using a single 10-μs π/2 pulse with a 0.5-s recycle delay. The [2]H_2O-containing samples were measured in flame-sealed 10-mm glass tubes (Wilmad Glass Co.). In determining the local order parameter for different phases as a function of temperature, the samples were allowed to equilibrate for 30 min at each temperature. Longer waiting periods resulted in no changes in the acquired ^{2}H NMR spectra.

In situ ^{13}C NMR measurements were performed on samples loaded into Kel-F inserts, specially designed for volatile materials, which fit into the 7.5-mm Chemagnetics MAS rotors. Carbon-13 NMR spectra were acquired under magic-angle spinning (MAS) conditions at 3 kHz, using a cross-polarization (CP) pulse sequence with π/2 pulses of 4−6 μs, CP contact times of 2.5 ms, high-power proton decoupling during detection, recycle delays of 5 s, and 600 scans.

Solution-state ^{29}Si NMR measurements were performed on the silicate precursor solutions and the aqueous-rich phase of the silicate−surfactant mesophase mixtures using 7-mm Kel-F vials with specially designed threaded caps that prevented material loss during heating. Magic-angle spinning (MAS) *in situ* [29]Si measurements were performed on the silicate−surfactant-rich phase of the mixtures at 3 kHz using Kel-F inserts. In all cases, single 5- to 6-μs π/2 pulses were applied with proton decoupling during detection, 30-s recycle delays, and 200−1500 scans (depending on the signal-to-noise ratio). Temperature-dependent [29]Si spin−lattice (T_1) relaxation measurements were conducted at 11.7 T, using inversion−recovery pulse sequences with recycle delays of 60−90 s, depending on the magnetic field strength and temperature, to ensure complete relaxation of [29]Si magnetization for all silicate species between each signal acquisition. Equilibrium distributions of silicate species in the aqueous precursor solution and in the silicate−surfactant liquid crystals were determined at different temperatures (following thermal equilibration for approximately 1 h) by integration and normalization of the various peaks in the one-pulse

(22) (a) Hauser, E. A.; Niles, G. E. *J. Phys. Chem.* **1941**, *45*, 954−959. (b) Shelton, R. S.; Van Campen, M. G.; Tilford, C. H.; Lang, H. C.; Nisonger, L.; Bandelin, F. J.; Rubenkoenig, H. L. *J. Am. Chem. Soc.* **1946**, *68*, 753−755.

(23) (a) Hendricks, W. M.; Bell, A. T.; Radke, C. J. *J. Phys. Chem.* **1991**, *95*, 9519−9524. (b) Knight, C. T. G. *Zeolites* **1989**, *9*, 448−450.

(24) Harris, R. K.; Knight, C. T. G. *J. Mol. Struct.* **1982**, *78*, 273−278.

^{29}Si NMR spectra. Bromine-81 NMR measurements were conducted using single 6-μs $\pi/2$ pulses, 0.5-s recycle delays, and 1000−2000 scans.

Small-Angle X-ray Scattering (SAXS). Silicate−surfactant mesophase and binary CTAB/H_2O mixtures were prepared either directly in 1.5- or 2.0-mm quartz capillaries (Charles Super Co.) or in small vials and subsequently transferred into the capillaries, which were then either flame-sealed or, for samples containing volatile compounds such as benzene or TMB, sealed with epoxy. The samples were equilibrated at 70 °C for at least 24 h before diffraction measurements were made. Under the conditions employed (pH 13), no silicate polymerization has been observed (see ^{29}Si NMR measurements below) nor is expected to occur.[25] Small-angle X-ray scattering experiments were performed using a variable-temperature X-ray sample holder with a rotating anode X-ray source ($\approx$13 kW) that produced 1.54-Å wavelength Cu Kα radiation. The data were collected on a MAR Research image plate detector with 0.01-Å^{-1} resolution. Plots of X-ray intensity versus scattering angle (2θ) were obtained by azimuthal averaging over the powder diffraction pattern.

Polarized Optical Microscopy (POM). Silicate−surfactant mesophase and binary 30 wt % CTAB/H_2O mixtures were equilibrated in an oil bath at 60−70 °C for at least 24 h prior to examination. The silicate−surfactant-rich phase of the two-phase multicomponent system and the one-phase CTAB/H_2O mixture were loaded into separate 0.05-mm × 1.0-mm × 50.0-mm borosilicate microslides (Vitro Dynamics Inc.) using capillary action aided by house-vacuum. The samples were then flame-sealed at both ends. A Nikon optical microscope (model OPTIPHOTO2-POL) was used in cross-polarized configuration to view the optical signatures produced by the defect structures within the silicate−surfactant mixtures. Samples were analyzed immediately after loading, as well as following an overnight annealing procedure at 50 °C using a hot-stage. Difficulties presented by overlapping defect patterns were mitigated by preparing thin samples (0.05-mm thickness), while defect densities in the plane of the microslide capillaries were reduced by the annealing treatment. This permitted the morphological assignment of the various optical textures observed for the silicate−surfactant mesophases, based on comparisons with the defect patterns of well-known mesophase structures.[26]

Theory

^{2}H NMR of Liquid Crystals. Deuterium (^{2}H) NMR measurements of deuterated surfactant species have been widely used to study lyotropic liquid crystal phase behavior, aggregate geometry (e.g., cylinders or sheets), local order parameters, and molecular motions.[27] Such information provides important insight on the molecular dynamics and organization of the organic component, which are examined here in detail for alkaline silicate−surfactant liquid crystal systems.

In a lyotropic liquid crystal, although molecular motion remains fast on the ^{2}H NMR time scale (10^{-5}–10^{-4} s), it is generally confined within the anisotropic geometry of the individual aggregates. This leads to a time-averaged value for the quadrupolar interaction that is non-zero. Consequently, the residual quadrupolar splitting in the spectrum yields information on the shape (including the asymmetry) of the aggregates and the average local order parameter of the C−[2]H bonds. For an isotropic distribution of liquid crystalline domains (i.e., a powder), the ^{2}H quadrupolar splitting between the two singularities of the Pake pattern is given by:[27]

$$\Delta\nu^{LC}_{powder} = |\delta \tfrac{1}{2}\langle 3\cos^2\theta_{PM} - 1\rangle_M \tfrac{1}{2}\langle 3\cos^2\theta_{MD} - 1\rangle_D| \quad (2)$$

δ is the anisotropy parameter given by $(^3/_4)(e^2qQ/h)$, where e^2qQ/h is the quadrupolar coupling constant (typically $\approx$125 kHz for a static aliphatic C−[2]H unit[27]). LC denotes a liquid crystal, while the terms in broken brackets $\langle\,\rangle$ refer to values that are time-averaged much faster than the NMR time scale. The angle θ_{PM} establishes the relative

(25) (a) Engelhardt, G.; Michel, D. *High Resolution Solid-State NMR of Silicates and Zeolites*; Wiley: New York, 1987. (b) Iler, R. K. *The Chemistry of Silica*; Wiley: New York, 1979.

(26) Hartshore, N. H. *The Microscopy of Liquid Crystals*; Microscope Publications Ltd.: London, 1974; p 49.

(27) Seelig, J. *Q. Rev. Biophys.* **1977**, *10*, 353−418.
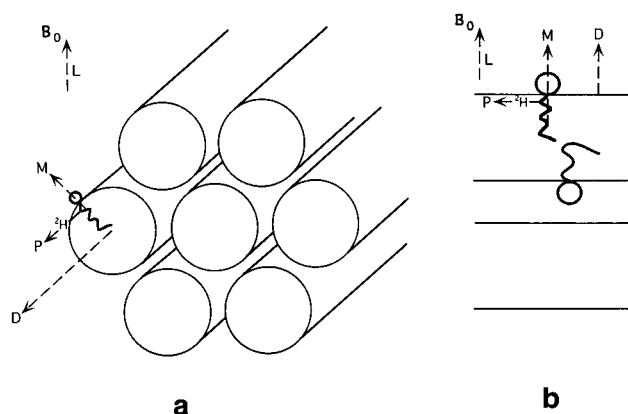
Figure 1. Definition of the four relevant coordinate systems used to describe (a) cylindrical and (b) planar liquid crystalline aggregates of self-assembled surfactant molecules, examples of which are schematically shown. The unique axis of the deuterium electric field gradient (EFG) (which corresponds to the C−[2]H bond axis) is defined by P, the z-direction of the surfactant molecular axis by M, and the z-direction of the director optical axis of an individual aggregate by D, which is parallel to the cylindrical axes in (a) or normal to the planar sheets in (b). The laboratory frame L is denoted by the direction of the applied magnetic field $\boldsymbol{B_o}$. For the two cases shown, local and translational motions of the surfactant molecules produce time-averaged electric field gradients, with their z-direction parallel to the director optical axes D of the aggregates.

orientations between a C−[2]H bond (P) and the surfactant molecular axis (M), as shown in Figure 1. The term $^1/_2\langle 3\cos^2\theta_{PM} - 1\rangle_M$ is often referred to as the local order parameter (S_{CD}) of the C−[2]H bonds. S_{CD} is generally temperature dependent and increases with decreasing temperature, reflecting increased local ordering as molecular mobility is reduced.[27] The term $^1/_2\langle 3\cos^2\theta_{MD} - 1\rangle_D$ depends on the angle θ_{MD} between the surfactant molecular axis (M) and the director optical axis of an individual aggregate (D), the latter being parallel to the cylindrical axes of aggregates in a hexagonal phase or normal to the bilayer planes of a lamellar phase (Figure 1). This term, thus, contains information on the aggregate geometry, being sensitive to lateral (i.e., translational) diffusion of surfactant molecules whose local orientations are time-averaged within a given aggregate.

The consequence of the rapid mobility of the surfactant molecules is that the unique axis (P) of the time-averaged quadrupolar interaction becomes parallel to the aggregate optical axis D. As shown in Figure 1, for a cylinder in a hexagonal (H_α) mesophase (Figure 1a, M⊥D), θ_{MD} is on average 90°, whereas for a bilayer plane in a lamellar (L_α) mesophase (Figure 1b, M ∥ D), θ_{MD} is on average 0°. For these two cases, eq 2 thus becomes

$$\Delta\nu^{H\alpha}_{powder} = \delta S_{CD}\left(\frac{1}{2}\right) \quad (3A)$$

and

$$\Delta\nu^{L\alpha}_{powder} = \delta S_{CD}(1) \quad (3B)$$

demonstrating that for equal order parameters (S_{CD}), a lamellar LLC phase is expected to yield a quadrupolar splitting that is twice as large as that for a hexagonal LLC morphology. Furthermore, for micellar phases or amphiphilic solutions that are below the critical micelle concentration (CMC), the surfactant molecules experience rapid and isotropic motions with respect to the laboratory frame ($\boldsymbol{B_o}$), with the result that $\langle 3\cos^2\theta_{PL} - 1\rangle_L$ is effectively averaged to zero on the time scale of the NMR measurement. Thus, the ^{2}H NMR spectra of micellar or sub-CMC solutions containing α-deuterated CTA$^+$ surfactant species consist of narrow isotropic peaks. Such conditions exist in the dilute (<20 wt % CTAB(aq)) micellar precursor solutions used to form the alkaline lyotropic silicate−surfactant liquid crystals described here.[5]

Results and Discussion

Under equilibrium conditions, alkaline silicate−surfactant mesophases fulfill the morphological and physicochemical
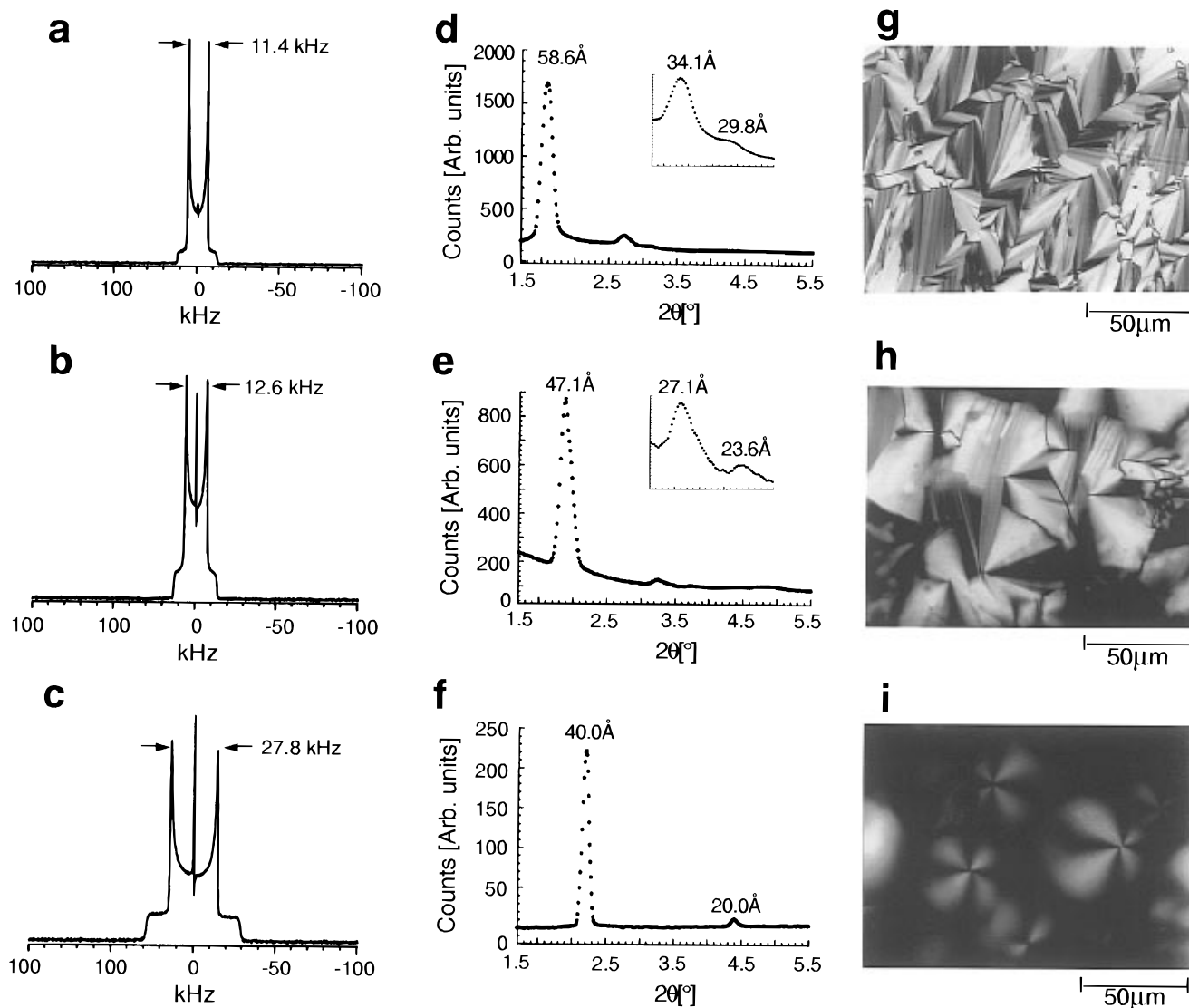
Figure 2. ^{2}H NMR spectra, small-angle X-ray scattering patterns, and polarized optical micrographs of typical binary CTAB/H$_2$O H$_\alpha$ and multicomponent H$_\alpha$ and L$_\alpha$ silicate−surfactant lyotropic liquid crystals (LLC). ^{2}H NMR spectra of CTA$^+$-d_2 (α-deuterated CTA$^+$) (a) in a 30 wt % aqueous solution at 30 °C in a hexagonal LLC phase ($\Delta\nu^{H_\alpha} = 11.4 \pm 0.1$ kHz), (b) in a hexagonal silicate−surfactant liquid crystal at 25 °C with an overall molar composition of 1.6SiO$_2$:207H$_2$O:1.32TMAOH:0.50CTAB:15.6CH$_3$OH ($\Delta\nu^{H_\alpha} = 12.6 \pm 0.1$ kHz), and (c) in a lamellar silicate− surfactant liquid crystal at 25 °C with an overall molar composition of 1.6SiO$_2$:207H$_2$O:1.32TMAOH:0.50CTAB:15.6CH$_3$OH:2.0C$_6$H$_6$ ($\Delta\nu^{L_\alpha} = 27.8 \pm 0.1$ kHz). The corresponding XRD patterns for each of these samples are shown in (d), (e), and (f), along with the d-spacings of the various peaks. Expansions of the d_{110} and d_{200} peaks are shown in the insets of (d) and (e). The corresponding cross-polarized optical micrographs for each of the samples at 50 °C are shown in (g), (h), and (i). The fan-shaped textures in (g) and (h) and the coarse mosaic pattern in (i) are typical defect patterns observed for hexagonal and lamellar liquid crystals, respectively.

criteria for classification as true lyotropic liquid crystals (LLCs). As complicated multicomponent systems, silicate−surfactant mesophases display rich phase behaviors that possess both clear similarities and striking differences to conventional CTAB/H$_2$O binary lyotropic liquid crystals. Results from complementary experimental techniques, such as NMR spectroscopy, X-ray diffraction, and polarized optical microscopy, in this comparative study provide detailed insight on the molecular and mesoscopic interactions governing the self-assembly and organization of silicate−surfactant mesophases. In this context, time- and composition-dependent phase transitions are examined quantitatively to establish the dominant molecular influences responsible for the different silicate−surfactant liquid crystal morphologies.

Characterization and Analyses of Silicate−Surfactant Liquid Crystal Phases. (a) Deuterium NMR. As described above, different lyotropic liquid crystal morphologies can be distinguished by line shape differences in their respective ^{2}H

NMR spectra. For example, Figure 2a displays the ^{2}H NMR spectrum for a binary CTAB/H$_2$O system at 30 °C, in this case an aqueous solution of 30 wt % CTAB deuterated at the α-carbon position (CTAB-d_2), which forms a well-known hexagonal (H$_\alpha$) LLC phase above its Krafft temperature (ca. 25 °C, for this composition).[28] In this nomenclature, the subscript α designates a high degree of alkyl chain mobility in terms of fast trans-gauche isomerization dynamics.[29] This mesophase consists of hexagonally packed cylindrical aggregates, with the aqueous and organic components forming continuous and discontinuous regions, respectively, within a given self-assembled domain (Figure 1a).[29] The H$_\alpha$ phase is a uniaxial system with its optical director axis D parallel to the axes of the cylinders. For the 30 wt % binary CTAB/H$_2$O

(28) Auray, X.; Petipas, C.; Anthore, R.; Rico, I.; Lattes, A. *J. Phys. Chem.* **1989**, *93*, 7458−7464.

(29) (a) Langevin, D. *Annu. Rev. Phys. Chem.* **1992**, *43*, 341−369. (b) Tiddy, G. J. T. *Phys. Rep.* **1980**, *57*, 1−46.

system, which exists in the weak-screening limit (i.e., in the absence of high electrolyte or salt concentrations), self-assembly and organization of aggregates are dominated by long-range repulsive inter-aggregate electrostatic forces. Under these circumstances, the system minimizes its total Gibbs free energy by arranging into ordered arrays of aggregates such that the inter-aggregate spacing is maximized. As a result, a single LLC phase is formed throughout the sample volume, consistent with the single Pake powder pattern possessing a $\Delta\nu_{powder}^{H\alpha} = 11.4 \pm 0.1$ kHz quadrupolar splitting shown in Figure 2a. By using eq 3A, along with the $\delta = \Delta\nu_{powder}^{static} = 112$ kHz measured in the ^{2}H spectrum (not shown here) of a random distribution of CTAB-d_2 crystals, the local order parameter is determined to be $S_{CD} = 0.204 \pm 0.002$.

Similarly, analyses of the ^{2}H NMR line shapes of more complicated multicomponent silicate−surfactant mixtures permit the geometrical shapes of aggregates in liquid crystal domains to be identified, along with the partitioning of deuterated species among different phases in the multiphase systems investigated here. Figures 2b and 2c show room temperature ^{2}H NMR spectra of two silicate−surfactant mesophase mixtures formed using α-deuterated CTAB-d_2 as the surfactant. The samples have identical compositions except for the presence of benzene, which was added as an organic solute to the mixture associated with Figure 2c to stabilize the lamellar mesophase. Under the experimental conditions employed in this study (e.g., silicate/ surfactant ratio, pH, temperature), the lamellar silicate−surfactant mesophase can only form when sufficient concentrations of organic solute molecules are present (see below). The ^{2}H quadrupolar splittings of these spectra ($\Delta\nu = 12.6$ and 27.8 kHz in Figures 2b and 2c, respectively) differ by approximately a factor of 2 and are comparable to the H_α and L_α phases of the binary CTAB/H_2O LLC systems. Referring to eq 3 and assuming similar (though not identical) order parameters for the two samples, the line shapes are attributed to hexagonal and lamellar silicate−surfactant liquid crystalline phases possessing cylindrical and flat sheet aggregate structures, respectively.[30] These assignments are confirmed by X-ray diffraction and optical microscopy measurements in Figure 2, which will be discussed below.

In contrast to the one-phase binary CTAB/H_2O system for which a H_α deuterium NMR powder pattern alone is observed (Figure 2a), the two-phase systems yield two prominent ^{2}H spectral features: one broad pattern from the mesoscopically ordered liquid crystal phase and another narrow signal from the isotropic water-rich phase. The relative fraction of the deuterated surfactant species in each of the phases is determined from the integrated peak areas of these features. The sharp peaks in the center of each spectrum in Figures 2b and 2c arise from the relatively small fraction of isotropically mobile surfactant species (ca. 4 mol % of the total CTA$^+$) that exist either as isolated molecules or in highly mobile micelles residing in the aqueous-rich phase (ca. 80 wt % of the total sample). Under the room-temperature alkaline conditions of this study, this surfactant-poor H_2O-rich phase is in thermodynamic equilibrium with the hexagonal or lamellar silicate−surfactant-rich liquid crystalline phase (Figures 2b and 2c, respectively), which accounts for the remaining ca. 20 wt % of the total sample mass and ca. 96% of the surfactant species in each of the two systems.

The coexistence of surfactant-poor isotropic and surfactant-rich liquid crystal phases within the multicomponent silicate− surfactant mixtures is characteristic of lyotropic systems in which attractive inter-aggregate forces dominate repulsive interactions. This is the case for the cooperative self-assembly process of silicate−surfactant mesophases,[5,6] in which the addition of multiply-charged anionic silicate oligomers in a highly basic solution to a dilute aqueous surfactant solution has been observed to form thermodynamically stable silicate− surfactant arrays. Though the aqueous silicate chemistry[25] and multicomponent phase equilibria are complex, the physics underlying the self-assembly process is common to lyotropic systems in general.

For example, the electrostatic forces between charged micellar surfaces are often treated using mean-field Poisson−Boltzmann (PB) theory[18] to understand the stabilities and phase behavior of self-assembled systems. In this framework, the presence of multiply-charged silicate anions in the inorganic electrolyte solution reduces the repulsive electrostatic inter-aggregate interactions in at least two ways. First, multiply-charged silicate anions reduce the effective Debye length associated with the charge repulsion among adjacent aggregates. This is because the magnitude of the Debye length, the characteristic length of the diffusive double layer, is inversely proportional to the charge of the electrolyte solute molecules.[18] Secondly, as the monovalent Br$^-$ anions are exchanged by the multiply-charged silicate species (see below), a higher association constant of the oligomeric silicate−surfactant complex is expected to diminish the surface potential of the aggregates. More quantitative assessment of the electrostatic interactions using the PB theory is limited by its continuum nature, which cannot easily accommodate the discrete charges and finite ion size effects[18] associated with the typically large oligomeric silicate anions.

In addition to the repulsive electrostatic forces between aggregates, attractive interactions exist in the form of short-range (r^{-6}) van der Waals forces among individual surfactant molecules (where r is the intermolecular distance). Assemblies of surfactant molecules, however, exhibit collectively longer range effects. For micelles or aggregates of surfactant species, the additivity of the van der Waals forces results in long-range interaction potentials that scale as d^{-1} or d^{-2} (where d is the inter-aggregate distance) between pairs of spherical or planar surfaces, respectively.[18] In contrast to the inter-aggregate repulsive interactions, which are highly dependent on aqueous solution conditions, the inter-aggregate attractive van der Waals forces are generally much less sensitive to variations in solution electrolyte concentrations or pH. (The exception to this generalization is the zero-frequency contribution which has electrostatic origins.[18]) In addition, attractive van der Waals-type ion-correlation forces are present among the highly polarizable and mobile silicate oligomers in the diffusive double layer surrounding the aggregates. The presence of micelles in the surfactant precursor solution, which promotes the existence of long-range van der Waals forces, appears to be an important prerequisite for self-assembly of aggregates to occur. Fully solvated surfactant monomers experience only short-range van der Waals interactions, which are expected to be insufficient to induce phase separation under the conditions used. In support of this, to our knowledge, no silicate−surfactant mesophases have been produced when the surfactant concentration in the precursor organic solution is below the CMC (0.0009 M for CTAB). Thus, the addition of highly anionic silicate species to an isotropic micellar CTA$^+$ solution shifts the overall force balance to favor attractive inter-aggregate interactions over diminished repulsive ones.

(30) The aggregate geometries have also been confirmed from ^{2}H NMR measurements made on CTA$^+$ species with perdeuterated trimethylammonium head groups, $C_{16}H_{33}N(C^2H_3)_3^+$. The hexagonal and lamellar silicate−surfactant liquid crystals, with compositions and conditions that are identical with those used in Figures 2b and 2c, exhibit ^{2}H quadrupolar splittings of 2.1 and 4.4 kHz, respectively, consistent with the geometries of the different phases (see eq 3).

The consequence of such prevailing attractive interactions is that the aggregates self-assemble and phase separation is induced, whereby one or more concentrated silicate−surfactant-rich phases adopt morphologies that minimize the total Gibbs free energy and establish a new equilibrium condition. It is important to add that the actual shapes of the micelles in the organic precursor solution are not directly relevant to the aggregate geometries in the resulting silicate−surfactant mesophases, because of the sizable influence that the silicate anions have on local and mesoscopic aggregate structures.[5] Under these circumstances, a relatively large-volume H_2O-rich isotropic phase is present containing soluble silicate, surfactant, cosolvent, and other electrolytes in dilute concentrations. The denser and more viscous silicate−surfactant-rich phases with accompanying solute components are comprised of aggregates that can organize into liquid crystalline arrays with long-range order.[5,6] That attractive inter-aggregate interactions are dominant furthermore suggests that the mean aggregate shape for the H_α silicate−surfactant liquid crystalline phase should be hexagonal, as indicated by transmission electron microscope measurements of polymerized MCM-41 mesoporous materials.[1b,3b,8c,13e] Direct measurement of this in the liquid crystalline materials here, however, is not possible, because rapid surfactant mobility obscures the distinction between hexagonal and cylindrical aggregate shapes within the sensitivity of the ^2H NMR experiments. In the absence of direct proof for a hexagonal aggregate shape in hexagonal silicate−surfactant liquid crystals, we will retain the "cylinder" label for the geometry of individual aggregates to avoid confusion with the hexagonal arrangement of these aggregates in the *p6mm* morphology.

Separate CP/MAS ^{13}C NMR experiments[6] have recently shown that the surfactant chain dynamics in silicate−surfactant and binary lyotropic liquid crystals are very similar, and that at room temperature, the silicate−surfactant mesophases are above their Krafft temperatures,[31] consistent with their liquid crystalline properties. These results validate the use of the subscript α (e.g., H_α and L_α), which designates the anisotropic liquid-like mobility of the alkyl CTA^+ chains in silicate−surfactant mesophases. Earlier work that sought to explain the phase separation of silicate−surfactant mesophases under moderately alkaline conditions (pH = 11) by hypothesizing Krafft temperatures above room temperature should be reexamined in light of these observations and the anticipated influence of silica polymerization. The phase separation of silicate−surfactant liquid crystals is related primarily to inter-aggregate interactions, namely attractive van der Waals forces, that dominate screened inter-aggregate repulsive electrostatic forces, rather than changes in intra-aggregate interactions, such as chain freezing below the Krafft temperature.

Comparison of the local order parameters in various liquid crystalline systems is useful for establishing the significance of the different molecular parameters and interactions within the constituent aggregates. For example, by using eq 3 in conjunction with the quadrupolar splittings in Figure 2, local order parameters in these hexagonal and lamellar silicate−surfactant mesophases at room temperature are evaluated to be $S_{CD} = 0.225 \pm 0.002$ and 0.248 ± 0.001 for the cylinder and sheet geometries, respectively. The slightly larger order parameter for the lamellar system is commonly observed in binary LLC systems and can be attributed to an overall smaller mean head-group area (a_o) available to each surfactant

molecule.[32a,33] This is accompanied by increased steric hindrance of the surfactant species and, consequently, a higher degree of local ordering of the ensemble of $C-^2H$ bonds. In addition, the larger value of the local order parameter of the silicate−surfactant hexagonal mesophase (0.225) compared to that of the binary $CTAB/H_2O$ LLC hexagonal phase (0.204 from above) is attributed to the different counterions in the two systems. In the former case, bulkier and more highly charged counterions, for example, double-four-ring (D4R) oligomeric silicate anions (with charges up to 8^-, depending upon pH),[34] can reduce the mobility of the cationic surfactant, increasing its order parameter in several ways. First, the high charge density of multiply-charged D4R anions at high pH results in strong ionic interactions with the cationic head groups. This produces more effective screening of the intra-aggregate electrostatic repulsions among surfactant species compared to monovalent anions such as Br^-, resulting in a smaller mean head-group area a_o (eq 1) for the silicate−surfactant complex. In addition, the multiply-charged anionic silicate species permit such interactions to take place with more than one cationic surfactant molecule, leading to what are essentially multiple-tailed silicate−surfactant complexes.[5,6] Such strong and multiple ionic interactions at the interface reduce the degrees of motional freedom available to the surfactant molecules, and ultimately to their constituent α-$C-^2H$ bonds via steric hindrance effects, leading to larger values for S_{CD} in these multicomponent systems.

(b) X-ray Diffraction. Whereas ^2H NMR characterizes the anisotropic mobility of surfactant molecules and thus the corresponding symmetry of individual aggregates, X-ray diffraction techniques probe the collective organization of such aggregates over longer length scales, typically 1−20 nm in the mesoscopic regime.[35] These measurements can be used to establish the morphology of a given mesophase and to quantify the dimensions of the liquid crystalline unit cell. Small-angle X-ray scattering (SAXS) techniques were therefore used to investigate the mesoscopic organization of multicomponent silicate−surfactant and binary $CTAB/H_2O$ lyotropic liquid crystals to complement the ^2H NMR measurements of local aggregate geometry.

Samples containing liquid crystalline domains with an isotropic distribution of orientations yield two-dimensional X-ray diffraction (XRD) patterns containing sets of rings that can be indexed to determine the morphology of the mesophase. Angle-dependent intensity plots averaged over the azimuthal angle are shown in Figures 2d, 2e, and 2f for the same 30 wt % CTAB/H_2O and silicate−surfactant mixtures whose ^2H NMR spectra are shown in Figures 2a, 2b, and 2c. The XRD pattern in Figure 2d of 30 wt % $CTAB/H_2O$ shows scattering intensity at $d_{100} = 58.6$ Å, along with the d_{110} and d_{200} scattering peaks at 34.1 and 29.8 Å (Figure 2d inset). This pattern has been indexed to a structure with *p6mm* hexagonal symmetry, which is consistent with the cylindrical aggregate geometry established by the ^2H NMR spectrum in Figure 2a and in close agreement with earlier XRD studies[36] that corroborate its H_α designation. The corresponding lattice parameter (i.e., the repeat distance between cylindrical aggregates $a_h = 2d_{100}/\sqrt{3}$) is $a_h = 67.7$ Å. Simi-

(31) Pershan, P. S. *J. Phys. Colloq.* **1979**, *4*, C3 423−432.
(32) (a) Charvolin, J.; Tardieu, A. *Solid State Phys.* **1978**, *14*, 209−257. (b) Marçelja. S. *Biochim. Biophys. Acta* **1974**, *367*, 165−176.

(33) Ekwall, P.; Mandell, L.; Fontell, K. *J. Colloid Interfac. Sci.* **1969**, *29*, 639−646.
(34) The pK_a values of the various silicate oligomers are not well established.[25b] Our calculations and measurements of pH indicate that, under the alkaline conditions employed, each D4R anion should possess at most a maximum charge of −6.
(35) Luzzati, V. In *Biological Membranes*; Chapman, D., Ed.; Academic Press: London, 1968; Vol. 1, pp 71−123.
(36) Fontell, K.; Khan, A.; Lindström, B.; Maciejewska, D.; Puang-Ngern, S. *Colloid Polym. Sci.* **1991**, *269*, 727−742.

larly, Figure 2e displays the XRD pattern of a silicate−surfactant mesophase indexed to a *p6mm* hexagonal structure, in this case with a *d*-spacing of $d_{100} = 47.1$ Å ($a_h = 54.4$ Å) and d_{110} and d_{200} peaks of 27.1 and 23.6 Å, respectively (see Figure 2e inset). These scattering data are consistent with the ^{2}H NMR spectrum (Figure 2b) of this material, which again corroborates its hexagonal H_α morphology. The inclusion of benzene in a mixture that is otherwise identical to the H_α silicate−CTA$^+$ mesophase above produces a dramatic change in the scattering pattern. The XRD pattern of this material is displayed in Figure 2f, providing clear evidence of a lamellar structure with a *d*-spacing of $d_{100} = 40.0$ Å and an accompanying d_{200} harmonic at 20.0 Å. The lamellar domains of this L_α silicate−surfactant mesophase are consistent with the planar aggregates established by the ^{2}H NMR measurements in Figure 2c.

Comparisons of the lattice parameters in the various liquid crystalline systems provide correlations between the underlying molecular-level interactions and their influences on the mesoscopic structural parameters. For example, the XRD d_{100}-spacings of the H_α and L_α silicate−surfactant liquid crystals (47.1 and 40.0 Å, respectively) are significantly larger than the corresponding d_{100}-spacings (40 and 35 Å, respectively[37]) of otherwise identical hexagonal and lamellar samples that were filtered and dried at room temperature. Water is removed from the silicate−surfactant-rich liquid crystal phases during the air-drying process, predominantly from the aqueous inorganic regions separating the aggregates. Because of this, molecular mobility is reduced and the samples are no longer liquid crystalline, though under these conditions they still retain mesoscopic hexagonal or lamellar morphologies.[37] This is consistent with the well-documented reduction of the hexagonal and lamellar unit cell (i.e., the lattice parameter) with decreasing water content in binary and ternary LLC systems, including those containing cationic CTAB.[36] The difference between the hexagonal silicate−surfactant and hexagonal binary CTAB/H$_2$O LLC mesophase d_{100}-spacings (47.1 and 58.6 Å, respectively) is explained by considering the dominating forces present in the two systems.[6] The attractive forces driving self-assembly of the silicate−surfactant liquid crystal phases produce lattice parameters that are substantially smaller than for repulsion-dominated single-phase LLC systems, in which inter-aggregate separations are maximized.[18]

(c) Polarized Optical Microscopy. On longer length scales, namely the wavelength of light, the mesophase morphologies can be characterized by polarized optical microscopy (POM),[26] the convenience of which will be helpful toward eventually establishing full multicomponent lyotropic silicate−surfactant phase diagrams. These measurements provide corroborative verification of the phase, which complement the molecular and mesoscopic ordering monitored by the ^{2}H NMR and SAXS techniques discussed above. In POM, characteristic optical patterns from different defect structures lead to mesophase-specific textures that can be used to identify different phase morphologies. In addition, the density of such defect structures in the patterns provides an estimate of the domain sizes within the liquid crystal phases. The POM texture of the binary 30 wt % CTAB/H$_2$O H_α LLC phase measured immediately after loading the material into a thin flat capillary contains dense striated nongeometric features (not shown) that reflect alignment of the mesophase produced by shear flow during the loading process.[37,38] By heating the sample to 50 °C and annealing

overnight, an angular fan-like optical pattern develops, as shown in Figure 2g, which is characteristic of the defect structure of a hexagonal mesophase.[38,39] Figures 2h and 2i display POM micrographs of hexagonal and lamellar silicate−surfactant liquid crystals, whose corresponding ^{2}H NMR spectra and XRD patterns in Figures 2b−c and 2e−f, respectively, have previously been discussed. The fan-like texture seen in Figure 2h is similarly observed after annealing the silicate−surfactant sample at 50 °C overnight and is again characteristic of a hexagonal mesophase. This is consistent with the ^{2}H NMR and XRD results in Figure 2b and 2e. The coarse mosaic texture shown in Figure 2i is typical of lamellar liquid crystals,[38,40] and thus is similarly consistent with the ^{2}H NMR and XRD results (Figures 2c and 2f), which in combination confirm a layered silicate−surfactant mesophase morphology. The lamellar defect pattern is observed after annealing, during which an initially fine mosaic pattern[37] transforms into the clear coarse mosaic texture with larger domain sizes (tens of micrometers). This demonstrates a principal processing advantage of preserving liquid crystalline properties prior to the polymerization of component species in inorganic−organic mesophase materials: greater control of domain growth permits much larger particle sizes to be produced than currently documented for hydrothermal synthesis procedures. The optical micrographs of the silicate−surfactant liquid crystals shown in Figures 2h and 2i are also the first demonstration that these mesophases have birefringent properties.

Interfacial Structure of Silicate−Surfactant Liquid Crystal Aggregates. Having thus established the liquid crystalline properties of silicate−surfactant mesophases under highly alkaline conditions in the absence of silica polymerization, control of molecular and mesoscopic structural features can be achieved by manipulating mixture composition and temperature. This is possible because of the direct effects that species concentration and solution temperature have on key intra- and inter-aggregate interactions, which are elucidated by molecular-level characterization of the organic−aqueous inorganic interface. Specifically, the local structures and dynamics of water, silicate anions, nascent counterions, organic solutes, polar cosolvents, and base species all contribute to the intra- and inter-aggregate interactions that are crucial to silicate−surfactant mesophase self-assembly and organization.

(d) Aqueous Solvent. On the hydrophilic side of the silicate−surfactant interface, ^{2}H, ^{29}Si, and ^{81}Br NMR measurements of deuterated water, the oligomeric silicate counterions, and the Br$^−$ counterions, respectively, provide complementary insights on the complicated aqueous silicate chemistry, which plays a key role in cooperative silicate−surfactant mesophase organization. As in the deuterated surfactant studies discussed above, ^{2}H NMR can be used to monitor deuterated water molecules from which the anisotropic dynamics of aqueous solvent species in the different liquid crystal phases can be established.[41] Figure 3a shows the ^{2}H NMR spectrum of ^{2}H$_2$O in the hexagonal 30 wt % CTAB/H$_2$O binary LLC phase at 40 °C. The observed 34-Hz quadrupolar splitting of the Pake pattern is in agreement with previously reported data[36] and is presented here to permit direct comparison with ^{2}H NMR data compiled for H$_2$O in the silicate−surfactant systems. Although the water molecules exchange rapidly at the surface of adjacent aggregates, their overall motion is nevertheless anisotropic, as evidenced by the small 34-Hz splitting and by the absence of

(37) Firouzi, A. Ph.D. Dissertation, University of California, Santa Barbara, manuscript in preparation.

(38) (a) Miller, C. A.; Ghosh, O.; Benton, W. *J. Colloid Surf.* **1986**, *19*, 197−223. (b) Bellare, J. R.; Davis, H. T.; Miller, W. G.; Scriven, L. E. *J. Colloid Interface Sci.* **1990**, *136*, 305−326.

(39) Rosevear, F. B. *J. Soc. Cosmet. Chem.* **1968**, *19*, 581−594.

(40) Lühmann, B.; Finkelmann, H.; Günther, R. *Makromol. Chem.* **1985**, *186*, 1059−1073.

(41) See, for example: (a) Blackburn, J. C.; Kilpatrick, P. K. *Langmuir* **1992**, *8*, 1679−1687. (b) Halle, B.; Wennerström H. *J. Chem. Phys.* **1981**, *75*, 1928−1943.
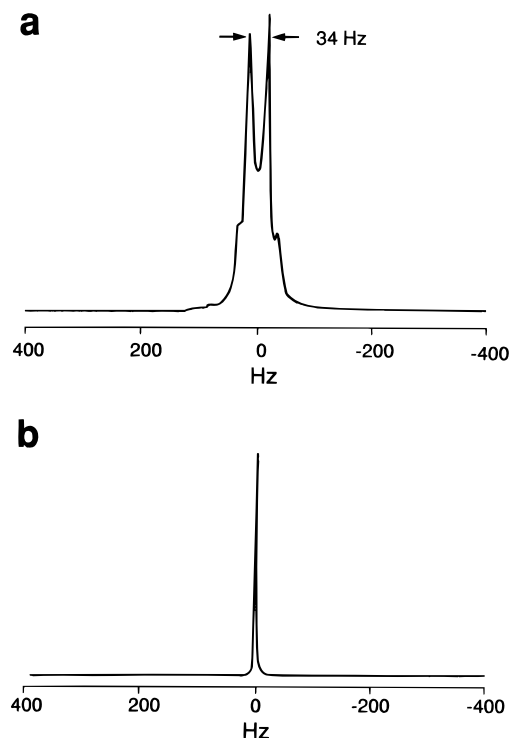
Figure 3. ^{2}H NMR spectra of ^{2}H$_2$O (a) in a binary 30 wt % CTAB/H$_2$O hexagonal LLC phase at 30 °C ($\Delta\nu^{H_\alpha} = 34 \pm 5$ Hz) and (b) in a hexagonal silicate−surfactant mesophase at 25 °C with an overall molar composition of 1.6SiO$_2$:207^{2}H$_2$O:1.32TMAOH:0.50CTAB:15.6CH$_3$OH.

an isotropic signal in the spectrum of Figure 3a for the single-phase 30 wt % binary CTAB/H$_2$O H$_\alpha$ liquid crystal. This is generally characteristic of water molecules in the aqueous regions of lyotropic liquid crystals in which repulsive electrostatic inter-aggregate interactions dominate mesophase self-assembly and organization.[18]

In contrast to the binary CTAB/H$_2$O H$_\alpha$ system, Figure 3b shows the room-temperature ^{2}H NMR spectrum of ^{2}H$_2$O in a two-phase hexagonal silicate−surfactant liquid crystal system, with a composition identical to the samples measured in Figures 2b, 2e, and 2h. The single isotropic peak is typical of all hexagonal or lamellar silicate−surfactant mesophases investigated here at high pH and at ambient temperatures and above. This indicates that during self-assembly and equilibration of the two-phase silicate−surfactant liquid crystal system, the water molecules are appreciably (though not totally) excluded from the silicate−surfactant-rich phase, within the sensitivity of the ^{2}H NMR measurement. In the aqueous-rich phase, the solvent water molecules experience a completely isotropic environment on the time scale of the NMR experiment.

(e) Counterion Species. The role of the various counterions in cooperative self-assembly of silicate−surfactant liquid crystals can be established using ^{29}Si and ^{81}Br NMR measurements of the oligomeric silicate and the Br$^-$ counterions, respectively. The crucial presence of highly-charged oligomeric silicate anions in alkaline inorganic precursor solutions has been shown to induce the self-assembly of silicate−surfactant mesophases.[1−9] As discussed above, this occurs because such species modify inter-aggregate interactions, with the result that attractive forces become dominant, and also influence intra-aggregate interactions, which govern the subsequent morphology. In particular, the rich compositional characters of aqueous silicate solutions provide an important means for influencing silicate−surfactant mesophase behavior. This is accomplished through manipulation of oligomeric silicate anion distributions and charge, which can be controlled by varying the solution conditions, for
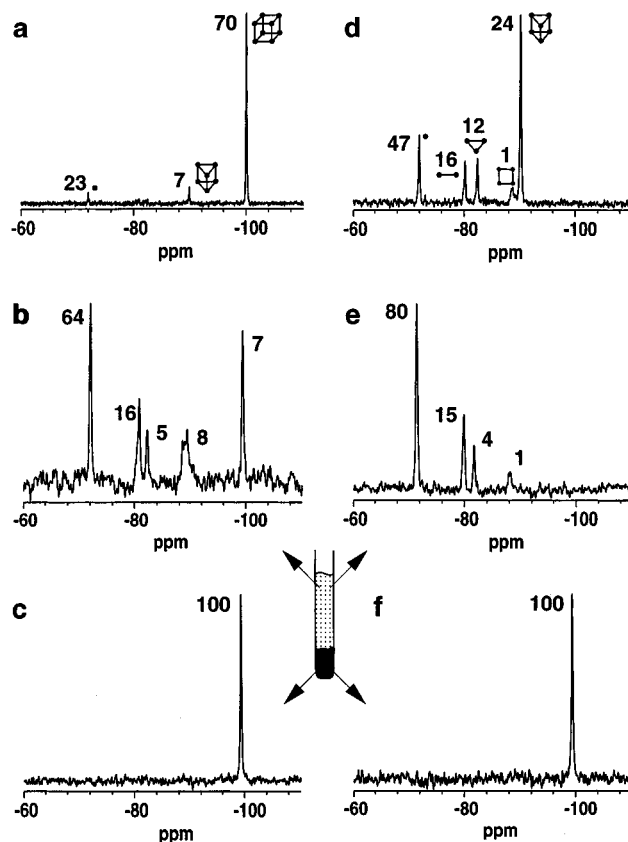
Figure 4. Room-temperature ^{29}Si NMR spectra of (a) a D4R-stabilized tetramethylammonium silicate precursor solution (pH 13.0) with a molar composition of 1.0SiO$_2$:1.1TMAOH:42.0H$_2$O:14.1CH$_3$OH, (b) the aqueous-rich phase and (c) the silicate−surfactant-rich phase that exist in equilibrium in the two-phase mixture formed after mixing the inorganic precursor solution in (a) to a 6.8 wt % CTAB(aq) solution, (d) a D3R-stabilized tetraethylammonium silicate precursor solution (pH 13.0) with a molar composition of 1.0SiO$_2$:3.7TEAOH:56.2H$_2$O: 12.3EtOH, (e) the aqueous-rich phase, and (f) the silicate−surfactant-rich phase that exist in equilibrium in the two-phase mixture formed after mixing the inorganic precursor solution in (d) to a 6.8 wt % CTAB(aq) solution. The ^{29}Si spectra shown in (a−b) and (d−e) were collected under solution-state conditions, whereas those in (c) and (f) employed MAS conditions to improve spectral resolution for the viscous liquid crystal samples. Separate ^{2}H NMR and XRD results show the silicate−surfactant-rich phases in (c) and (f) to be hexagonal liquid crystals. The various ^{29}Si peaks in the spectra are assigned to the different silicate anion species, based on their isotropic chemical shifts.[25a] The mole percents of the various silicate species reported in the text are obtained by dividing the respective integrated ^{29}Si peak areas by the number of Si nuclei in the corresponding silicate oligomer and then normalizing.

example, the cation type (e.g., alkali metal or tetraalkylammonium species) of the base, pH, Si/OH ratio, temperature, or the concentration of alcohol co-solvent additives or hydrolysis byproducts.[42]

The distribution of silicate species in such multicomponent mixtures can be quantitatively determined through the use of *in situ* ^{29}Si NMR measurements.[23,24,25a] The ^{29}Si solution-state NMR spectrum in Figure 4a, for example, shows peaks corresponding to the different oligomeric silicate species that exist in a typical inorganic precursor solution used for the preparation of silicate−surfactant liquid crystals. In this

(42) (a) McCormick, A. V.; Bell, A. T. *Catal. Rev.−Sci. Eng.* **1989**, *31*, 97−127. (b) Kinrade, S. D.; Swaddle, T. W. *Inorg. Chem.* **1988**, *27*, 4253−4259. (c) Hasegawa, I.; Kuroda, K.; Kato, C. *Chem. Soc. Jpn.* **1986**, *59*, 2279−2283. (d) Groenen, E. J. J.; Kortbeek, A. G. T. G.; Sudmeijer, O.; Mackay, M. *Zeolites* **1986**, *6*, 403−411. (e) Hendricks, W. M.; Bell, A. T.; Radke, C. J. *J. Phys. Chem.* **1991**, *95*, 9513−9518.

mixture, the double-four-ring (D4R) silicate oligomer $[Si_8O_{20}H_n]^{(8-n)-}$ has been stabilized by using tetramethylammonium hydroxide (TMAOH) as the source of base and methanol as a co-solvent. Under the high pH conditions employed, silicate species are highly ionized,[23] so that n will generally be a small integer number. Integration of the various [29]Si peaks in Figure 4a establishes that 4% of the [29]Si nuclei belong to silicate monomers ($SiO_4H_n^{(4-n)-}$ at −72.4 ppm), 6% to double-three-ring (D3R) units ($Si_6O_{15}H_n^{(6-n)-}$ at −90.0 ppm), and 90% to double-four-ring (D4R) units ($Si_8O_{20}H_n^{(8-n)-}$ at −99.9 ppm). Normalized with respect to the number of Si atoms in each species, the precursor silicate solution is determined to contain an equilibrium mixture in molar percentages of 23% monomers, 7% D3R species, and 70% D4R species.

Previous work has suggested that during the self-assembly of silicate−surfactant liquid crystals the anionic silicate oligomers compete with and ion exchange for the monovalent Br^- and OH^- counterions.[5,6] By examining the partitioning of various silicate species between the isotropic aqueous-rich and liquid crystalline silicate−surfactant-rich phases, insight is obtained on the molecular features of the anion species that promote mesophase formation under different conditions. Addition of the silicate precursor solution in Figure 4a to an isotropic 6.8 wt % micellar CTAB solution induces the self-assembly of a silicate−surfactant-rich mesophase, under these conditions an H_α liquid crystal phase, which separates from and coexists with an aqueous-rich phase.[43] To analyze the partitioning of the silicate counterions among these different phases, the two were separated by gentle centrifugal action and analyzed independently, yielding the ^{29}Si NMR spectra in Figures 4b and 4c for the aqueous-rich and silicate−surfactant-rich phases, respectively. The dramatically different distributions of silicate anion species in the two phases show there to be strong ion-correlation preferences between certain silicate anions and the cationic CTA^+ head group. For example, based on the solution-state and MAS ^{29}Si NMR spectra in Figures 4b and 4c, respectively, the aqueous-rich phase contains large mole fractions of monomers (64%) and dimers (16%) (Figure 4b), while the silicate−surfactant-rich phase possesses exclusively D4R oligomers (100%) (Figure 4c). Preferential incorporation of the double-ring silicate species into the silicate−surfactant liquid crystal mesophase can be explained by the different interactions experienced by oligomeric and monomeric anions with the aqueous solvent and charged surfactant head groups. The smaller silicate anions, such as the monomer, dimer, and cyclic trimer units, are expected to possess higher charge densities and consequently larger hydration spheres, leading to higher solubilities in water compared to the D4R structures.[44] In addition, electrostatic repulsions between adjacent surfactant head groups will hinder complexation of small silicate anions to more than one bulky CTA^+ species. Furthermore, at pH conditions higher than 13.5, for which *in situ* ^{29}Si NMR measurements show the resulting silicate−surfactant mixture to contain only monomeric (85%) and dimeric (15%) silicate anions,[45] no mesophase self-

assembly occurs at all.[37] The absence of mesophase self-assembly in the presence of predominantly monomeric silicate anions at extremely high pH conditions illustrates the important role played by the larger oligomeric silicate species (e.g., doubling-ring structures) in inducing phase separation of silicate−surfactant mesophases.

Following mesophase self-assembly, information on the mobility of the double-ring silicate anions in the liquid crystal materials is provided by ^{29}Si NMR spectra acquired in the absence of magic-angle spinning. For example, a static ^{29}Si NMR measurement of the hexagonal silicate−surfactant-rich liquid crystal phase yields a spectrum (not shown)[37] with a slightly broader line width (2 ppm) for the D4R species compared to that in Figure 4a (0.1 ppm) for the dilute silicate precursor solution. This is consistent with the less efficient motional averaging of the D4R [29]Si chemical shift tensors in the liquid crystal, due to strong interactions between the double-ring silicate anions and the surfactant head groups at the inorganic−organic interface. Nevertheless, the 2-ppm [29]Si line width is much narrower than the 79-ppm chemical shift anisotropy for a closely related polycrystalline solid D4R silicate−tetramethylammonium hydrate,[46] which indicates that the interfacial silicate species in the liquid crystal remain rapidly mobile on the time scale of the NMR measurement. This characteristic is common to liquid crystalline materials in which the counterions possess a high degree of mobility within the aqueous interstitial region.[18]

The equilibrium distributions of silicate anions in the alkaline precursor and liquid crystal solutions are influenced significantly by the base cations and by the presence of alcohol co-solvent species. For example, whereas tetramethylammonium hydroxide (TMAOH) and methanol have been shown to stabilize D4R silicate species under ambient conditions at high pH,[23,24] the use of tetraethylammonium hydroxide (TEAOH) and ethanol stabilizes the D3R (and smaller) units, as evidenced by the dominant signal from D3R species at −90.0 ppm in Figure 4d. From the normalized integrated [29]Si peaks, this silicate precursor solution contains an equilibrium mixture of 47% monomers ($SiO_4H_n^{(4-n)-}$ at −72.4 ppm), 16% dimers ($Si_2O_7H_n^{(6-n)-}$ at −81.0 ppm), 12% cyclic trimers ($Si_3O_9H_n^{(6-n)-}$ at −82.7 ppm), 1% cyclic tetramers ($Si_4O_{12}H_n^{(8-n)-}$ at −88.2 ppm), and 24% D3R species ($Si_6O_{15}H_n^{(6-n)-}$ at −90.0 ppm), in molar percentages. Addition of this precursor solution to an isotropic 6.8 wt % micellar CTAB solution yields an aqueous-rich isotropic phase and a silicate−surfactant-rich H_α phase, whose solution-state and MAS ^{29}Si NMR spectra are shown in Figures 4e and 4f, respectively. Again, the various silicate oligomers are partitioned differently among the two phases at equilibrium: the aqueous-rich phase contains large concentrations of monomers (80%), as well as dimers (15%), cyclic trimers (4%), and cyclic tetramers (1%) (Figure 4e), while the silicate−surfactant-rich phase possesses exclusively D4R units (100%) (Figure 4f).

The shift in the distribution of double-ring anions from the D3R oligomers in the silicate precursor solution (Figure 4d) to the D4R units in the silicate−surfactant-rich phase (Figure 4f) has been studied by *in situ* MAS ^{29}Si NMR measurements and is shown in a series of time-resolved spectra in Figure 5. Although the peak at −90.0 ppm in Figure 5a demonstrates that the D3R oligomers are initially incorporated into the hydrophilic region of the silicate−surfactant-rich mesophase, their relative concentration diminishes with time in favor of the D4R units (Figures 5b−5f). The presence of the trimethylam-

(43) Addition of a similar highly alkaline precursor solution *without* silicate counterion species does not induce self-assembly and phase separation of silicate−surfactant-rich mesophases. Although high-pH conditions alone (in the absence of silicate anions) are expected to reduce inter-aggregate electrostatic repulsive forces, the inter-aggregate van der Waals attractive interactions are apparently not strong enough to produce the net attractive forces necessary for self-assembly to occur. As a result, the surfactant aggregates (i.e., micelles) at high pH remain in solution, as verified by ^{2}H NMR measurements.[37]

(44) Wijnen, P. W. J. G.; Beelen, T. P. M.; de Haan, J. W.; van de Ven, L. J. M.; van Santen, R. A. *Colloids Surf.* **1990**, *45*, 255−268.

(45) The mixture had an overall molar composition of 1.0SiO₂:207H₂O: 3.9NaOH:0.10CTAB.

(46) Grimmer, A. R.; Peter, R.; Fechner, E.; Molgedey, G. *Chem. Phys. Lett.* **1981**, *77*, 331−335.

3606   *J. Am. Chem. Soc., Vol. 119, No. 15, 1997*

Firouzi et al.
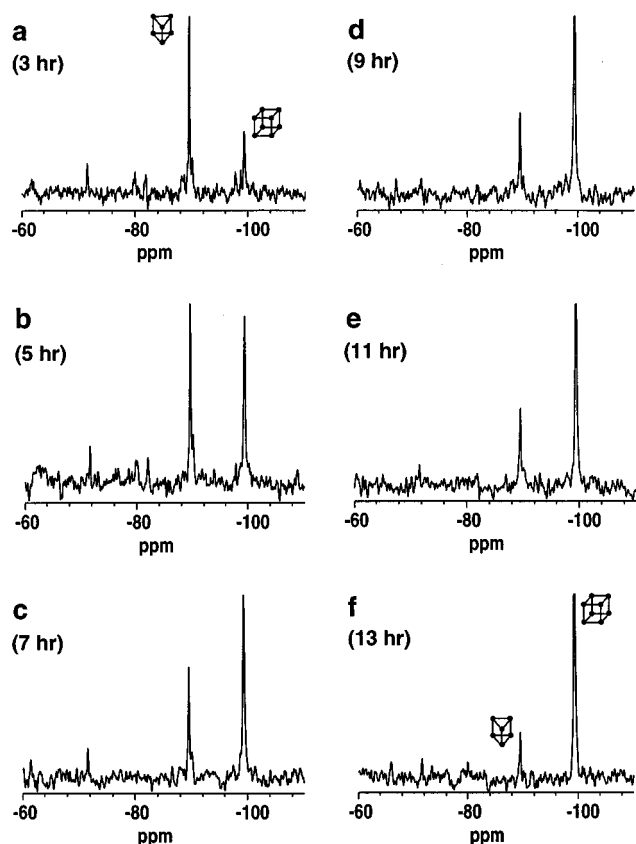
Figure 5. Room-temperature *in situ* MAS ^{29}Si NMR spectra of the hexagonal silicate−surfactant-rich phase formed after mixing the D3R-stabilized inorganic precursor solution in Figure 4d with a 6.8 wt % CTAB(aq) solution. The spectra were acquired at different times shown after the point of initial mixing. The D4R mole fractions, D4R/(D4R + D3R), are established by integrating the respective peaks in the ^{29}Si spectra yielding (a) 0.25, (b) 0.48, (c) 0.61, (d) 0.67, (e) 0.74, and (f) 0.88.

monium cation moiety in the CTA$^+$ surfactant molecule is apparently responsible for the stabilization of the D4R silicate oligomers in the silicate−surfactant liquid crystals. The stability of the D4R units under similar conditions has been previously established and ascribed to the formation of hydrated clathrate-like structures, where the anionic double-ring silicate species are surrounded by charge-compensating TMA$^+$ cations and are additionally stabilized by hydrogen bonding to water and alcohol solvent molecules.[47]

The crucial role of the surfactant head group in stabilizing certain oligomeric silicate anions at the hydrophilic−hydrophobic interface is confirmed by examining the effect of different head group moities on the silicate anion distribution in the liquid crystal phases. Moreover, provided sufficient concentrations of multiply-charged oligomeric silicate anions are present to initiate mesophase self-assembly, the ultimate equilibrium distribution of anions in the silicate−surfactant liquid crystals does not depend strongly on the species distribution in the silicate precursor solution. For example, addition of an inorganic precursor solution formed using tetraethoxysilane (TEOS) and NaOH, which is known to contain a variety of silicate species,[44,47] to a 6.8 wt % CTAB solution yields a H$_\alpha$ silicate−surfactant liquid crystal that coexists with an aqueous-rich phase.[48] The *in situ* MAS ^{29}Si NMR spectrum of the

equilibrated silicate−surfactant-rich H$_\alpha$ phase is identical to Figures 4c and 4f, verifying the stabilizing influence of the CTA$^+$ head group on the D4R structures at the hydrophilic−hydrophobic aggregate interface.[37] Separately, addition of a D4R-stabilized inorganic precursor solution (containing TMAOH and CH$_3$OH) to an aqueous surfactant precursor solution containing 8.5 wt % octadecyl*triethyl*ammonium bromide, [C$_{18}$H$_{37}$N$^+$(CH$_2$CH$_3$)$_3$]Br$^-$ (C$_{18}$TEABr), yields a silicate−surfactant mesophase[49] whose ^{29}Si NMR spectrum (not shown here) contains predominantly D3R oligomers.[37] Thus, despite the absence of any D3R units in the initial silicate precursor solution, the triethylammonium head group of C$_{18}$TEABr causes the equilibrium silicate distribution to shift toward D3R oligomeric species. These results demonstrate clearly that the structure of the cationic surfactant head group exerts a strong preference for certain oligomeric silicate species. This shifts the equilibrium anion distribution accordingly at the hydrophilic−hydrophobic interface, irrespective of the base cation and, to a significant extent, the composition of the silicate precursor solution. This is valid for the pH range 11.8 < pH < 13.5 and solution conditions where highly charged double-ring silicate oligomers (e.g., D4R and D3R units) are present to interact with the cationic surfactant head groups and thereby induce the self-assembly of a silicate−surfactant liquid crystal phase.

The process of ion-exchange of the monovalent Br$^-$ anions for the multiply charged silicate oligomers can be semiquantified using ^{81}Br NMR measurements. In the fast-motion limit, the ^{81}Br NMR line width of solvated bromide ions experiencing an averaged electric field gradient (EFG) environment is known to scale as $q^2\tau_c$, where q is the z-component of the EFG and τ_c is the correlation time for its fluctuations.[50] For the case where the bromide ions are exchanging among several distinct sites with residence times much smaller than the relaxation time, the observed line width is given by $\Delta\nu_{obs}^{fwhm} = \sum_i p_i \Delta\nu_i^{fwhm}$, where $\Delta\nu_i^{fwhm}$ and p_i are the line width and time-averaged occupancy probability, respectively, for Br$^-$ anions in a given site i. For example, the ^{81}Br NMR spectrum in Figure 6a, acquired at 30 °C for a binary 30 wt % CTAB/H$_2$O hexagonal LLC phase, shows a line width of $\Delta\nu_{obs}^{fwhm} = 10$ kHz, in good agreement with earlier values in the literature.[50] A simple two-site model has been previously proposed for this system,[50] in which the Br$^-$ anions exchange rapidly between two environments, namely, (i) Br$^-$ in close association with the cationic surfactant (p_s) and (ii) water-solvated Br$^-$ in aqueous solution (p_w). On the basis of the degree of association of bromide ions to CTA$^+$ at room temperature,[51] p_s is approximately 0.8 and therefore $p_w \approx 0.2$. Taking $\Delta\nu_w^{fwhm} = 360$ Hz, as measured for a 8 wt % aqueous NaBr solution, $\Delta\nu_s^{fwhm}$ is estimated to be ca. 12.4 kHz.

By comparison, the ^{81}Br NMR spectrum of a silicate−surfactant mesophase mixture, containing both hexagonal (H$_\alpha$) silicate−surfactant-rich and isotropic aqueous-rich phases, is shown in Figure 6b similarly to possess a single peak, though with a substantially narrower line width of $\Delta\nu_{obs}^{fwhm} = 2$ kHz. Upon separation of the two phases, the ^{81}Br NMR spectrum of the H$_\alpha$ silicate−surfactant-rich phase reveals no signal whatsoever, while that of the aqueous-rich phase is identical, both in line shape and in total intensity, to that shown in Figure 6b.

(47) (a) Wiebcke, M.; Hoebbel, D. *J. Chem. Soc., Dalton Trans.* **1992**, *16*, 2451−2455. (b) Wiebcke, M.; Grube, M.; Koller, H.; Engelhardt, G.; Felsche, J. *Microporous Mater.* **1993**, *2*, 55−63.

(48) The mixture had an overall molar composition of 1.0SiO$_2$:164H$_2$O: 2.0NaOH:0.11CTAB.

(49) The mixture had an overall molar composition of 1.0SiO$_2$:218H$_2$O: 0.82TMAOH:0.62C$_{18}$TEABr:9.8CH$_3$OH.

(50) (a) Lindblom, G.; Lindman, B.; Mandell, L. *J. Colloid Interface Sci.* **1973**, *42*, 400−409. (b) Lindblom, G.; Lindman, B.; Mandell, L. *J. Colloid Interface Sci.* **1970**, *34*, 262−271.

(51) Evan, D. F.; Miller, D. D. In *Water Science Review*; Franks F., Ed.; University Press Cambridge: London, 1989; Vol. 4, pp 1−39.
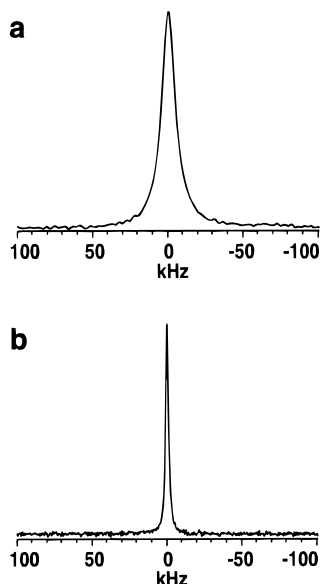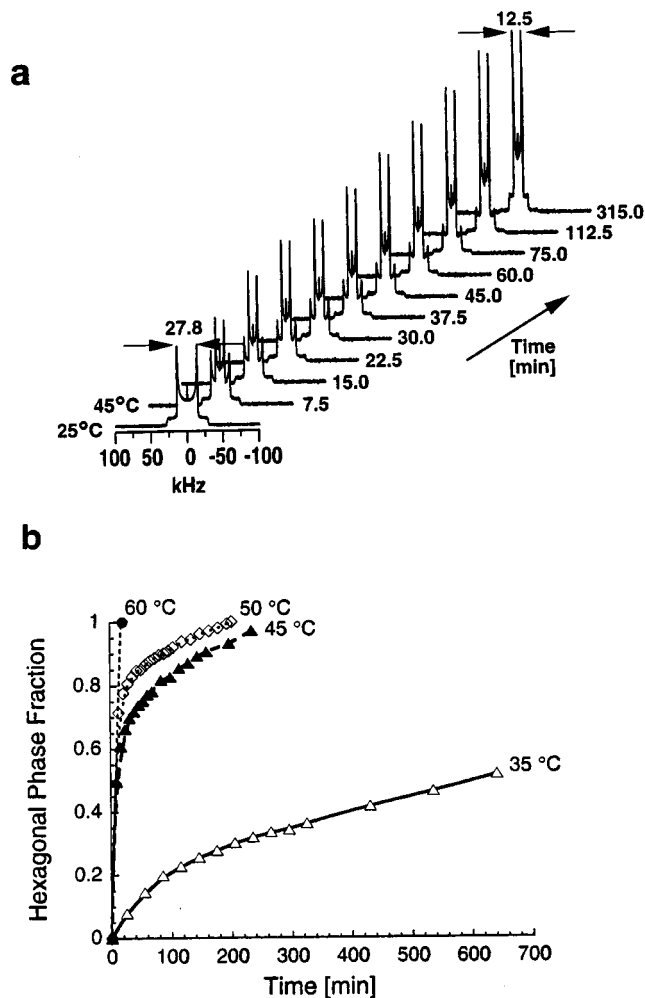
Figure 6. Solution-state ^{81}Br NMR spectra of (a) a binary 30 wt % CTAB/H_2O hexagonal LLC phase at 30 °C ($\Delta\nu_{obs}^{fwhm} = 10.0 \pm 0.1$ kHz) and (b) a silicate−surfactant mesophase mixture containing both hexagonal silicate−surfactant-rich and isotropic aqueous-rich phases at 25 °C with an overall molar composition of 1.6SiO_2:207H_2O: 1.32TMAOH:0.50CTAB:15.6CH_3OH ($\Delta\nu_{obs}^{fwhm} = 2.0 \pm 0.1$ kHz).

These observations and elemental analysis results[52] establish that within experimental sensitivity, virtually all bromide anions have been exchanged for the silicate oligomers, which preferentially interact with the CTA$^+$ head groups. Moreover, separate ^{81}Br NMR experiments suggest that the 2-kHz line width of the aqueous-rich phase is consistent with bromide anions associated with tetramethylammonium cations from the TMAOH base source.[37] The partitioning of halide (e.g., Br$^-$) and inorganic (e.g., silicate) counterions between the different phases is central to the liquid crystal self-assembly process in these multicomponent inorganic−surfactant mesophase systems. For the case at hand, aggregate interfaces are altered by strong interactions between the cationic CTA$^+$ head groups and multiply charged double-ring silicate anions, which effectively shield inter-aggregate electrostatic repulsions and thereby induce phase separation.

Silicate−Surfactant Liquid Crystal Phase Transformations. At equilibrium, the aqueous-rich and silicate−surfactant-rich phases discussed above adopt morphologies that derive from complicated force balances among numerous competing intra- and inter-aggregate interactions, which result in a system with the lowest overall free energy. By manipulating the system variables, such as temperature and composition, the molecular parameters and corresponding interactions, most importantly at the interface, can be modified to exert appreciable control over transformations between different silicate−surfactant mesophases.

The time and temperature dependence of liquid crystal phase transitions can be quantified using *in situ* ^{2}H NMR measurements in conjunction with spectral simulations.[41a] For example, the collection of ^{2}H NMR spectra shown in Figure 7a shows the time-resolved transformation of a lamellar silicate−surfactant mesophase, similar to the one characterized in Figures 2c, 2f, and 2i, into a hexagonal morphology. Such a transformation occurs when the temperature of the system is increased, in this

(52) The elemental analysis results in wt % are as follows: silicate− surfactant-rich phase: 52.6% C, 6.5% Si, and 0.0% Br (below detection limit); aqueous-rich phase: 5.9% C, 0.7% Si, and 1.0% Br. Hydrogen and oxygen account for the remaining composition fractions.

Figure 7. (a) Time-resolved ^{2}H NMR spectra of a lamellar silicate− surfactant mesophase transforming into a hexagonal morphology. After a step-change in temperature from 25 to 45 °C, the initial lamellar mesophase (first slice, $\Delta\nu^{L_\alpha} = 27.8$ kHz) converts into a hexagonal phase over 4 h. (b) The fraction of the total ^{2}H NMR line shape contributed by the hexagonal silicate−surfactant mesophase as a function of time after a step change in temperature of 35 ($\triangle$), 45 ($\blacktriangle$), 50 ($\diamond$), and 60 °C ($\bullet$), as obtained from line-fitting simulations of time-resolved spectra (e.g., Figure 7a). The rate of this phase transformation is observed to be strongly temperature dependent. The mixture had an overall molar composition of 1.4SiO_2:196H_2O: 1.0TMAOH:0.50CTAB-d_2:18.8CH_3OH:1.2TMB.

case by a step change from 25 to 45 °C.[5] The lamellar mesophase, which exists at room temperature, yields a ^{2}H NMR spectrum (Figure 7a, first slice) with a quadrupolar splitting of $\Delta\nu^{L_\alpha} = 27.8$ kHz that is identical to that in Figure 2c. After the temperature is increased to 45 °C, superimposed Pake patterns with quadrupolar splittings of $\Delta\nu^{L_\alpha} = 27.8$ kHz (lamellar phase) and $\Delta\nu^{H_\alpha} = 12.5$ kHz (hexagonal phase) are jointly present and easily discernible. Such superposition of line shapes is consistent with the coexistence of randomly oriented distributions of lamellar and hexagonal domains during the transformation and is also characteristic of a first-order process.

Each time-resolved spectrum can be deconvoluted using line-fitting simulations to quantify the separate contributions of the isotropic aqueous phase and the lamellar and hexagonal liquid crystalline phases at different times during the silicate− surfactant mesophase transition.[53] Based on such simulations

(53) Firouzi, A.; Schaefer, D. J.; Tolbert, S. H.; Stucky, G. D.; Chmelka, B. F. Manuscript in preparation.

(not shown explicitly here), Figure 7b displays the relative fraction of the hexagonal phase present in the silicate−surfactant-rich material as a function of time during the lamellar-to-hexagonal phase transformation. The rate of this phase transition, the origin of which will be discussed in more detail below, is found to be strongly temperature dependent, occurring more rapidly at higher temperatures.

Moreover, in the absence of polymerization of the silicate species, the lamellar-to-hexagonal phase transformation is completely reversible, although a strong hysteresis is observed in the rate at which the reverse hexagonal-to-lamellar transition occurs. For example, for a 25-to-60 °C step change in temperature, the L_α-to-H_α transition takes place within 0.3 h, whereas for a 60-to-25 °C step change in temperature, the reverse H_α-to-L_α transformation requires over 4 h to complete.[37] These observations are explained by considering the various terms in eq 1, which predicts the equilibrium aggregate structure based on the relative magnitude of molecular parameters. One possible explanation for the observed phase transformation involves the temperature-dependent solubility of the organic solute species, in this particular case trimethylbenzene (TMB), which increase the effective volume V of the hydrophobic regions of the aggregates. In addition, the temperature-dependent equilibrium distribution of silicate counterions can alter the electrostatic shielding among charged species at the aggregate interface, which will influence the mean-head-group area a_o and the effective volume V of the surfactant molecules. Both the organic solute concentration and the distribution of silicate anions can, thus, affect the local curvature of the aggregate, as registered by a change in the packing parameter g, to a point where either the cylindrical geometry, flat-sheet structure, or other morphology is preferred.

(f) Organic Solute Effects. A combination of ^{13}C, ^2H, and ^{29}Si NMR techniques establishes the dominating molecular events that lead to mesoscopic phase transitions in alkaline silicate−surfactant liquid crystals. For example, high-resolution CP/MAS ^{13}C NMR measurements allow the roles of different organic solute species in the phase transformation process to be monitored. In particular, the sensitivity of the ^1H−^{13}C dipole−dipole coupling to molecular mobility allows the efficiency of the cross-polarization process to be used as a probe of different molecular environments.[54] Figure 8a displays room-temperature CP/MAS ^{13}C NMR spectra from a silicate−surfactant mesophase sample, whose lamellar morphology has been previously established and well characterized (Figures 2c, 2f, and 2i). The peaks are assigned to the following carbon species:[55] aliphatic −CH$_2$− methylene groups in the alkyl surfactant chain (33 ppm), methyl groups associated with the −N(CH$_3$)$_3^+$ trimethylammonium head group of the surfactant (55 ppm), and aromatic carbon atoms in solute benzene species (130 ppm). These moieties, namely the methylene groups of the alkyl surfactant chain and the methyl units of the trimethylammonium head group, and the benzene solute species experience sufficiently constrained mobility to preserve ^1H−^{13}C dipole coupling and thus possess reasonable CP efficiencies.

Variable-temperature CP/MAS ^{13}C NMR measurements show that the lamellar-to-hexagonal phase transformation (e.g., Figure 7a) coincides with expulsion of the organic solute species from the hydrophobic regions of silicate−CTA$^+$ aggregates. As the
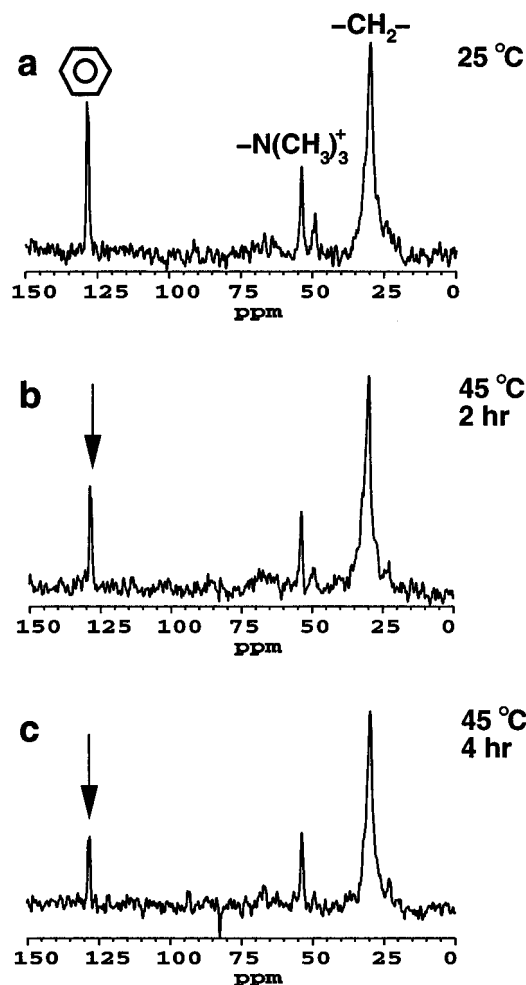
Figure 8. Room-temperature CP/MAS ^{13}C NMR spectra before and after a step change in temperature from 25 to 45 °C, after which an initially lamellar silicate−surfactant liquid crystal transforms into a hexagonal morphology (e.g., Figure 7a). (a) The lamellar mesophase mixture initially at 25 °C and the transforming mixture (b) 2 h and (c) 4 h after the temperature of the sample was raised to 45 °C. The sample possessed an overall molar composition of 1.6SiO$_2$:207H$_2$O:1.32TMAOH:0.50CTAB:15.6 CH$_3$OH:2.0C$_6$H$_6$.

temperature is increased to 45 °C, the relative intensity of the benzene ^{13}C peak at 130 ppm decreases with time, as shown in Figures 8b and 8c after 2 and 4 h, respectively.[56] Over the moderate temperature range examined, it is reasonable to assume that the CP efficiencies of the different organic groups will possess approximately equivalent temperature dependences, thereby allowing qualitative comparisons among spectral features that have been normalized to the intensity of their respective −CH$_2$− group signals. The reduced CP ^{13}C NMR signal from benzene in Figures 8b and 8c is consistent with the diminished solubility of benzene in paraffinic liquids with increasing temperature and the resulting depletion of solute benzene species from the organic region of the liquid-crystalline aggregates.[57] Upon entering the H$_2$O-rich phase, the solvated benzene molecules experience rapid isotropic mobility with typical rotational correlation times on the order of 10^{-11} s. Such rapid motion diminishes significantly the efficiency of $^1H \rightarrow {}^{13}C$ cross-polarization for benzene molecules that have

(54) (a) Pines, A.; Gibby, M. G.; Waugh, J. S. *J. Chem. Phys.* **1972**, *56*, 1776−1777. (b) Bovey, F. A.; Jelinski, L. W. *J. Phys. Chem.* **1985**, *89*, 571−583. (c) Schaefer, J.; Stejskal, E. O.; Buchdahl, R. *Macromolecules* **1977**, *10*, 384−405. (d) Sindorf, D. W.; Maciel, G. E. *J. Am. Chem. Soc.* **1983**, *105*, 1848−1851.

(55) Ulmius, J.; Lindman, B.; Lindblom, G.; Drakenberg, T. *J. Colloid Interface Sci.* **1978**, *65*, 88−97.

(56) After 6 h the benzene ^{13}C peak intensity was unchanged compared to that in Figure 8c. As each ^{13}C spectrum took 2 h to acquire, this indicates that at 45 °C the redistribution of benzene molecules between the aqueous-rich and silicate−surfactant-rich phases had reached equilibrium some time during the $t = 2−4$ h time interval.

(57) Jada, A.; Lang, J.; Zana, R. *J. Phys. Chem.* **1990**, *94*, 381−387.
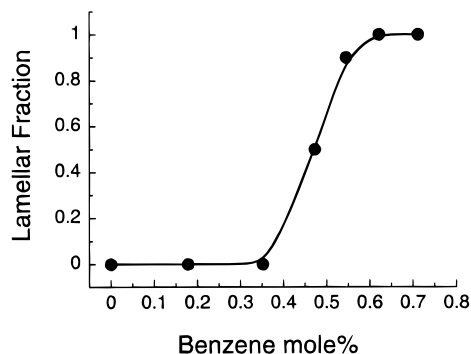
Figure 9. The dependence of the lamellar fraction of various silicate−surfactant mesophases on the concentration of benzene solute species in mixtures with otherwise constant overall molar compositions of $1.6SiO_2$:$207H_2O$:$1.32TMAOH$:$0.50CTAB$-d_2:$15.6CH_3OH$, obtained from the deconvolutions of the resulting room-temperature ^2H NMR spectra. Measurements are accurate to within ±0.025 for the lamellar fraction and within ±0.01 mol % for the benzene composition (smaller than the symbols shown).

been expelled from the liquid crystal aggregates, with the result that the relative ^{13}C NMR signal is reduced in intensity (Figures 8b and 8c). Cooling the silicate−surfactant mesophase back to 25 °C increases the solubility of benzene molecules in the hydrophobic region of the aggregates, which nevertheless requires 6 h to restore the benzene CP/MAS ^{13}C NMR signal intensity to what it was initially in Figure 8a. The rate of benzene re-incorporation is slow compared to its expulsion due to the entropic barriers and mass transport limitations that must be overcome to re-concentrate the benzene solute species in the hydrophobic mesophase aggregates from the dilute aqueous-rich phase.

The direct connection between the lamellar−hexagonal silicate−surfactant phase transformation and the expulsion/re-incorporation of the organic solute is confirmed by ^2H NMR measurements on a series of silicate−surfactant liquid crystal samples in which all component concentrations and conditions were kept constant, with the exception of benzene, which was varied systematically from 0 to 0.71 mol %. Figure 9 summarizes the deconvolutions of the resulting room-temperature ^2H NMR spectra of α-deuterated CTA$^+$ surfactant species (similar to those in Figure 7a), which quantify the normalized contributions of the lamellar and hexagonal silicate−surfactant mesophase domains. For benzene concentrations up to 0.35 mol %, the sample contains only hexagonal phase domains. However, as the bulk benzene concentration is varied from 0.35 to 0.62 mol %, the lamellar fraction increases progressively from zero to unity at the expense of the hexagonal phase. At higher concentrations (ca. 0.70 mol %), solely a lamellar morphology is observed. The step-function-like change from purely hexagonal to purely lamellar phase over the narrow range (0.27 mol %) of benzene concentration indicates that a threshold local concentration of organic solute species is apparently required to increase the effective hydrophobic volume V to a level where the flat sheet geometry is preferred over a cylindrical or hexagonal aggregate shape. Further support for the role of the organic solute in stabilizing the lamellar mesophase is provided by the addition of benzene to an existing hexagonal silicate−surfactant liquid crystal: 8 h after adding benzene (to obtain 0.71 mol %) to a room-temperature hexagonal mesophase ($\Delta\nu^{H_\alpha}$ = 12.5 kHz) the sample had transformed completely to a lamellar phase ($\Delta\nu^{L_\alpha}$ = 27.8 kHz). Under the experimental conditions employed in this study (e.g., silicate/surfactant ratio, pH, temperature), it was possible to form the lamellar silicate−surfactant mesophase only when sufficient concentrations of
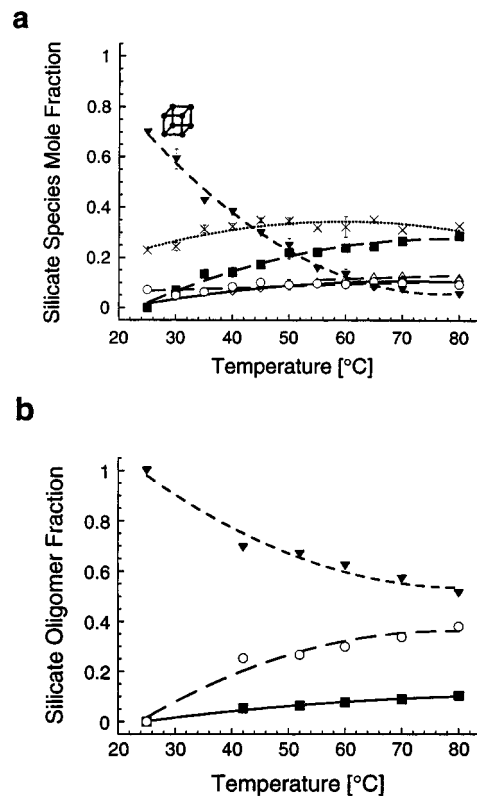
Figure 10. The equilibrium distributions of various silicate species (as determined from ^{29}Si NMR measurements) as a function of temperature (a) in the aqueous inorganic precursor solution (pH 13.0) with a molar composition of $1.0SiO_2$:$1.1TMAOH$:$42.0H_2O$:$14.1CH_3$-OH, expressed as mole fractions of total silicate species (×, monomer; ■, dimer; ◇, cyclic trimer; △, cyclic tetramer; ○, D3R; and ▼, D4R) and (b) in the lamellar silicate−surfactant mesophase mixtures with an overall molar composition identical to the sample used in Figure 8, expressed as fractions of silicate structural units (■, Q^1 species and Q_3^2 cyclic trimers from −79 to −81 ppm; ○, other Q^2 species and Q_6^3 D3R units from −81 to −92 ppm; and ▼, other Q^3 species including Q_8^3 D4R oligomers from −95 to −101 ppm).[59] The lines have been added to guide the eye.

organic solute molecules, such as benzene or TMB, were present. These results and analyses are corroborated as well by separate ^2H NMR measurements of deuterated benzene in aligned silicate−surfactant liquid crystal systems.[37]

(g) Temperature-Dependent Silicate Anion Distributions. In addition to the temperature-dependent solubility influences of organic solute species, temperature-dependent changes in the distribution of inorganic anion species can also contribute to the phase behavior of silicate−surfactant liquid crystals. For example, as discussed above, the various silicate species interact differently with the CTA$^+$ head group, so that a change in the relative anion concentrations can be expected to alter the balance of forces at the hydrophilic−hydrophobic interface and thereby influence self-assembly and mesophase organization. Focusing first on the silicate precursor solution, anion distributions in initially double-ring-stabilized mixtures are significantly modified at higher temperatures. Figure 10a shows the normalized redistribution of equilibrium silicate anion concentrations that occurs as a function of temperature in the initially D4R-stabilized aqueous silicate precursor solution (Figure 4a) at high pH (13.0), as determined from solution-state ^{29}Si NMR measurements. As the temperature is increased, the D4R oligomers decompose into smaller silicate units, such as monomers, dimers, cyclic trimers, and/or D3R species, presumably due to disruption of the ionic or hydrogen bonding interactions that stabilize the

D4R structures, as discussed above. These observations are consistent with previous investigations that have documented the instability of the D4R silicate oligomers at higher temperatures in basic solutions of tetramethylammonium hydroxides.[25a,58]

Similar trends exist for the redistribution of the silicate species in alkaline silicate−surfactant mesophase mixtures, as shown in Figure 10b. These data are from *in situ* MAS ^{29}Si NMR measurements made on the same sample whose lamellar-to-hexagonal phase transformation was monitored in Figure 7 using ^{2}H NMR. For these measurements, particularly at higher temperatures, a distribution of the silicon chemical shift environments broadens the ^{29}Si NMR peaks and thus specific assignments (e.g., cyclic trimer, D3R) of the resonance lines are difficult. In contrast to the silicate precursor solution, the double-ring structures (Q^3 species,[59] which include D4R and D3R silicate oligomers) display improved stability at higher temperatures, which is attributed to the stabilizing influence of the strongly interacting CTA^+ head group, as discussed previously. Nevertheless, at higher temperatures, smaller silicate anions (Q^1 and Q^2 species) form at the expense of the double-ring oligomers. The smaller anions impart less effective screening of electrostatic repulsions among CTA^+ molecules, yielding an increase in the mean head-group area a_o. This results in a decrease in the packing parameter g compared to conditions favoring D4R or D3R silicate species (see eq 1). A consequence of this is that redistribution of the silicate species concentrations at higher temperatures toward smaller anions may enhance the local curvature of the aggregate and thereby contribute to the observed lamellar-to-hexagonal phase transformation discussed above. However, this does not appear to be the dominant factor in producing the phase change, as the temperature-dependent distributions of the different silicate species in both the inorganic precursor solution and the silicate−surfactant mesophase are found to be fully reversible with no temperature-dependent hysteresis in the rate of response. These results are comparable with previous infrared and NMR measurements made on aqueous tetramethylammonium silicate solutions.[58] The strong hysteresis observed in the rate of the silicate−surfactant mesophase transformation, thus, indicates that the effects of silicate anion redistribution are small compared to the influence of the organic solute species over the range of mixture compositions and conditions examined in this study.

Conclusions

Comprehensive chemical and structural characterizations of alkaline lyotropic hexagonal and lamellar silicate−surfactant

liquid crystals have been obtained with the use of NMR, small-angle X-ray diffraction, and polarized optical microscopy. The use and applicability of such corroborative techniques have been key to establishing the effects of different molecular parameters on liquid crystal properties and phases, which are complicated by the multicomponent characteristics of these systems. In the absence of silica polymerization, silicate−surfactant mesophases can be prepared with liquid crystalline properties that are analogous to conventional binary and ternary LLC systems. The governing interactions in the self-assembly of alkaline lyotropic silicate−surfactant liquid crystal phases are attractive inter-aggregate forces, which induce separation of silicate−surfactant-rich and aqueous-rich phases. By using unreactive silicate species at high pH and ambient temperatures, the silicate−surfactant self-assembly process has thus been decoupled from the kinetics of interfacial silicate polymerization. Moreover, by manipulating molecular parameters, and thus implicitly the intra- and inter-aggregate interactions through control of solution composition and conditions, reversible transformations between phases can be induced. Molecular packing criteria have been used to guide experimental measurements that account for composition- and temperature-dependent structural changes in silicate−surfactant mesophases over molecular, mesoscopic, and macroscopic length scales. The resulting insights have important implications for mechanisms of self-assembly and structure direction in numerous closely related multicomponent inorganic−organic or hydrophilic−hydrophobic systems, such as zeolites, mesoporous materials, and biominerals. In general, effects from simultaneous and often transient thermodynamic, chemical reaction, and mass transport phenomena must be separated to establish and effectively control synthesis and processing variables with the aim of improving macroscopic material properties.

(58) See, for example: Groenen, E. J. J.; Emeis, C. A.; van den Berg, J. P.; de Jong-Versloot, P. C. *Zeolites* **1987**, *6*, 474−477.

(59) $Q^{\,y}_{\,z}$ denotes a Si atom with y connectivity (i.e., y-coordinated SiO_4^{4-} tetrahedra), and z (when applicable) indicates the number of equivalent atoms in the symmetric anion.